Weak-field magnetoresistance and substrate-induced strain in (111)-oriented PbTe films

R. S. Allgaier
Naval Surface Weapons Center, White Oak, Silver Springs, Maryland 20910
and Theodore Associates, Inc., 10510 Streamview Court, Potomac, Maryland 20854
(Received 14 June 1984)

Rotational weak-field magnetoresistance (WFMR) measurements were carried out at 300, 77, and 4.2 K on four (111)-oriented n-type PbTe films, deposited by hot-wall epitaxy on BaF_2. The results were analyzed in terms of a four-coefficient generalization of the Seitz-Pearson-Suhl formulation of WFMR which can detect symmetry-lowering effects. Film thicknesses ranged from 4 to 16 μm, carrier densities from 6×10^{16} to 1×10^{17} cm^{-3}, and carrier mobilities from about 1400 at room temperature to as high as 500 000 cm^2/V sec at 4.2 K. For each of 48 runs, WFMR data were obtained as the magnetic field $\vec{B}$ was rotated in the (111) film plane and in a plane perpendicular to the film. The expected sinusoidal behavior is skewed in the second case (the extrema do not occur at special orientations of $\vec{B}$ imposed by crystal symmetry), so that all four coefficients of the generalized theory, b, c, d, and d', were determined in each case from measurements on the same sample. For cubic symmetry, $d'=d$, but it was generally found that $d'<d$ at all three temperatures and decreases with decreasing temperature. This increasing film distortion (an in-plane extension) was ascribed to the thermal-expansion-coefficient difference between the PbTe film and its BaF_2 substrate. The deviations from $d'/d=1$ are smaller in one sample which had been repeatedly cycled between 300 and 4.2 K during an earlier study. For the other three samples at 4.2 K, the measurements yielded $d'/d\approx10^{-2}$ and a longitudinal WFMR that is an order of magnitude smaller than that found in bulk PbTe. These unique characteristics suggest that all, or essentially all, of the carriers from the four $\langle 111\rangle$-oriented valleys of the PbTe conduction band had been transferred to the single valley normal to the film plane. The sets of four WFMR coefficients from each run conform closely to the symmetry constraint imposed by a trigonally distorted, three-parameter version of the magneto-transport model for the cubic $\langle 111\rangle$ multivalley band structure. Values of the carrier transfer parameter F in this model provide more quantitative information about the shift of carriers into the single valley. The other two parameters—the valley mobility anisotropy K and scattering factor G—are generally similar to values found in bulk crystals at 300 and 77 K, but for two of the four films exhibit unreasonable increases at 4.2 K. Ultimately, these were attributed to the enhancement of the WFMR when the magnetic field is perpendicular to the film plane, an effect which is probably associated with stress relaxation across the film thickness. Finally, the values of F were used to deduce that the intervalley energy shifts increase from about 3 meV at 300 K to 12 meV or more at 4.2 K, corresponding to calculated tensile strains in the film plane of 0.4 and 1.6×10^{-3}. Smaller tensile strains at 4.2 K, and zero or even compressive strains at 300 K, have been deduced from other kinds of measurements. A complete explanation for these substantial differences is lacking, but it seems evident that two important factors are the preparation conditions and the thermal history of each sample.

I. INTRODUCTION

There are three weak-field magnetoresistance (WFMR) coefficients in the more commonly studied classes of cubically symmetric crystals.[1] They may be determined from measurements on one sample in three suitably chosen configurations. Their anisotropy, or symmetry, has been used to determine the band-edge electronic structures in many semiconductors, especially those of the multivalley type, where the symmetry conditions are simple and very sensitive to the valley orientation.[2] The traditional analysis of WFMR data always begins by considering theoretical models which are consistent with the crystallographic symmetry normally associated with the material under investigation. We[3] recently pointed out, however, that it is possible to carry out four potentially independent WFMR measurements on one sample with a fixed current orientation, and to distinguish alternative possible crystallographic or electronic symmetries from any relationships that may be found among the four coefficients.[4–7] Preliminary measurements[8,9] suggested that this four-coefficient (4C) WFMR technique could become a convenient, reliable, and sensitive tool for detecting symmetry-lowering effects in oriented films and layers.

This paper presents the results of the first extended series of measurements based on the 4C WFMR technique. The emphasis here is on *rotational* WFMR, i.e., on its behavior as the magnetic field is rotated at fixed magnitude in various planes. The data were obtained at 300, 77, and 4.2 K on (111)-oriented films of n-type PbTe, epitaxially deposited on BaF_2 using the hot-wall method.[10] The results were used to detect and analyze the effects of

substrate-induced strain on the PbTe films, and demonstrate that it is possible to detect strains as small as 1×10^{-4}. Some selected results from the complete study were described earlier in a brief letter.[11]

The IV-VI compound semiconductor PbTe crystallizes in the cubic NaCl structure. Its electronic structure is characterized by a narrow, direct forbidden energy gap at the four equivalent L points of the Brillouin zone.[12] Thus the constant-energy surfaces near the extrema of both the conduction and valence bands consist of cubically symmetric arrays of four $\langle 111\rangle$-oriented ellipsoids of revolution. The earliest evidence favoring this type of band-edge structure in PbTe came in fact from WFMR measurements on n- and p-type crystals.[13–17]

It is now firmly established that epitaxial films of PbTe and other IV-VI semiconductors can be prepared with a number of basic properties which are close to those characterizing high-quality bulk samples.[18,19] Some differences between film and bulk properties also have been detected, measured, and analyzed,[18] but they do not necessarily imply lower film quality. About 20 years ago, for example, it was reported that (100)-oriented films of PbS, PbSe, and PbTe, epitaxially deposited on NaCl, exhibited optical-absorption edges at 77 K corresponding to energy gaps that were 15—30 meV smaller than bulk values.[20,21] This decrease was ascribed to an in-plane compression of the films, due to the integrated effect of the difference in thermal-expansion coefficients of film and substrate between 300 and 77 K.

Additional band-structure alterations may be anticipated in (111)-oriented PbTe films since, unlike the (100) case, substrate strain will remove the energy degeneracy of the four L-point band edges. In 1978 Shubnikov—de Haas measurements on a (111)-oriented n-type PbTe film on BaF_2 revealed that at 4.2 K all of the carriers (6×10^{16} cm^{-3}) had been transferred to the single valley normal to the film plane.[22] This was shown to be a reasonable result, since the estimated strain of 2×10^{-3} and Ferreira's calculated deformation potentials for PbTe (Ref. 23) predicted a valley energy shift of 30 meV, approximately three times the one-valley Fermi level at that carrier density. In contrast to the earlier results for PbTe on NaCl, the thermal-expansion-coefficient difference leads in this case to an in-plane expansion of the film, corresponding to an "antibismuth" kind of trigonal distortion.

Since 1978, several kinds of measurements have provided additional evidence for the presence of a significant tensile strain in PbTe/BaF_2 at 4.2 K.[24–30] At room temperature on the other hand, a 1976 x-ray study of (111)-oriented PbTe found no strain, to within the experimental uncertainty of 3×10^{-5}, for films deposited on BaF_2 or SrF_2.[31] But in 1982, x-ray measurements on PbTe/BaF_2 at room temperature detected substantial in-plane *compressive* strains in the range $-(0.3–1.0)\times10^{-3}$.[32,33] The compression was ascribed to the elastic retention of up to about 3% of the 4% lattice mismatch between PbTe ($a=6.460$ Å) and BaF_2 ($a=6.200$ Å).

The specific reason for carrying out the present series of measurements was to use the 4C WFMR technique to obtain information about the state of strain in PbTe/BaF_2 at both low and high temperatures. A more general purpose was to provide a thoroughly documented example which could serve as an evaluation of the potential value of this new technique. Consequently, what follows is a very detailed analysis of an unusually large collection of WFMR measurements. This may be somewhat of an overreaction to my recognition that many of the older conventional WFMR studies on cubically symmetric semiconductors tend to be fragmentary and incomplete, including our own early results on bulk n-type PbTe.[16] I believe this reflects the time-consuming tedium that had to be endured in order to acquire highly precise and accurate sets of WFMR data. The unfortunate consequence is that it is often difficult to evaluate the accuracy of published WFMR data on semiconductors or their sensitivity to various perturbations.

In any case, Sec. II provides a thorough review of previously published two- and three-coefficient (2C,3C) WFMR measurements on PbTe, both n- and p-type and mostly bulk material, and compares the results to the general WFMR phenomenology for cubic crystals and to the standard $\langle 111\rangle$ ellipsoidal multivalley transport model. Section III describes the characteristics of the newer 4C WFMR phenomenology for the case of (111)-oriented films and layers, outlines the previously published derivation of a trigonally distorted $\langle 111\rangle$ multivalley transport model based on that 4C phenomenology, and summarizes measurements from the only two published experimental studies (both on n-type PbTe on BaF_2) which have utilized the 4C WFMR technique. Section IV describes the more or less conventional experimental procedures and equipment used, as updated by the addition of a modern computer system for the acquisition, processing, storage, and display of the experimental data. Section V presents and analyzes the results from 48 WFMR runs, each involving about 10^3 individual measurements. The WFMR coefficients from 11 selected runs are plotted, and for all runs are tabulated and fitted to the general 4C phenomenology and to the specific trigonal model mentioned above. Explanations for the sample-to-sample and run-to-run variations in the tabulated results are considered. An extended discussion of the unusual characteristics of the WFMR measurements at 4.2 K is included in this section. Finally, the intervalley carrier-transfer factors obtained from fitting the WFMR coefficients to the trigonally distorted multivalley transport model are used to obtain information about valley band-edge energy shifts and substrate-induced strain in the PbTe films between 300 and 4.2 K, and these are compared to the corresponding results obtained from other types of published measurements. Section VI presents the conclusions derived from this long study, with regard to the specific and general motivations for carrying it out.

II. WFMR IN CUBIC PbTe

The WFMR coefficients in this paper will be presented as dimensionless quantities M_{ϕ}^{θ}, defined by the relation

$$\Delta\rho/\rho_0=M_{\phi}^{\theta}(\mu_H\,|\,\vec{\mathbf{B}}\,|\,/C)^2\,, \tag{1}$$

where $\Delta\rho/\rho_0$ is the fractional change in the zero-field resistivity ρ_0, ϕ and θ specify the directions of sample

current and magnetic field, μ_H is the Hall mobility ($\mu_H = R_H/\rho_0$, where R_H is the weak-field Hall coefficient), $\vec{B}$ is the applied magnetic field, and C is the electric-magnetic compatibility factor.

For the more highly symmetrical types of cubic symmetry,[1] Seitz[34] and Pearson and Suhl[35] showed that M_ϕ^θ in any configuration may be written in the compact form

$$M_\phi^\theta = b + c\left[\sum_s \iota_s \eta_s\right]^2 + d\sum_s \iota_s^2 \eta_s^2 , \tag{2}$$

where b, c, and d will henceforth be referred to as the Seitz-Pearson-Suhl (SPS) WFMR coefficients, and ι_s and η_s are the direction cosines of the sample-current and magnetic field directions *in the cubic axis coordinate system*. This equation predicts that when $\vec{B}$ is rotated in any plane, at fixed magnitude, sinusoidal behavior with 180° periodicity will result.

In the case of PbTe, which cleaves along (100) planes, it is easiest to prepare a sample with the current along a [100] axis. Using Eq. (2) leads to

$$M_{100} = b + c + d \tag{3}$$

(the absence of a superscript on M_ϕ^θ will henceforth identify a *longitudinal* WFMR coefficient, for which $\theta = \phi$) and

$$M_{100}^{001} = M_{100}^{\perp} = b . \tag{4}$$

The $\perp$ superscript stands for *any* direction perpendicular to [100]. Because of this degeneracy, Eqs. (3) and (4) provide the only measurable combinations of the SPS coefficients, and therefore c and d cannot be separately determined from WFMR measurements on such a sample.[36] The most common method of determining b, c, and d individually in PbTe and other cubic semiconductors is to use a [110]-oriented sample and measure the longitudinal coefficient

$$M_{110} = b + c + \tfrac{1}{2}d \tag{5}$$

and the two *non*equivalent transverse coefficients

$$M_{110}^{001} = b \tag{6}$$

and

$$M_{110}^{1\bar{1}0} = b + \tfrac{1}{2}d . \tag{7}$$

Note that these three coefficients are extrema with respect to the rotational WFMR in the planes formed by each pair of them, i.e., the extrema are determined by crystallographic symmetry, not by the values of b, c, and d. We will sometimes refer to such 2C and 3C sets of WFMR data on cubic crystals, based on Eqs. (3) and (4) and Eqs. (5)–(7), respectively, as incomplete and complete.

To relate these configurations traditionally used on bulk samples with the present measurements on (111)-oriented films, I will also mention three rarely used configurations with $\vec{B}$ in two perpendicular directions *in* the (111) plane and in the [111] direction *normal* to it, viz., the longitudinal configuration

$$M_{1\bar{1}0} = b + c + \tfrac{1}{2}d , \tag{8}$$

the transverse in-plane coefficient

$$M_{1\bar{1}0}^{11\bar{2}} = b + \tfrac{1}{6}d , \tag{9}$$

and the transverse normal coefficient

$$M_{1\bar{1}0}^{111} = b + \tfrac{1}{3}d . \tag{10}$$

Although it is not obvious from Eq. (2), it can be shown that the WFMR in these three specific configurations remains the same for all directions of sample current in the (111) plane.

The SPS formulation of WFMR turned out to be especially convenient for the classification of the cubically symmetric, ellipsoid-of-revolution multivalley models. For this kind of band structure, it was discovered that a simple, linear WFMR symmetry condition of the form

$$b + c + xd = 0 \tag{11}$$

is satisfied, with $x = 1$, 0, and -1, when the valley symmetry axes lie along the ⟨100⟩, ⟨111⟩, and ⟨110⟩ directions, respectively.[37,38] Only the first two structures have been found in actual semiconductors, simply because cubic symmetry does not require rotationally symmetric valleys in the third case.[39]

The reduction from three to two independent WFMR coefficients imposed on these multivalley models by Eq. (11) reflects the fact that b, c, and d may all be expressed in terms of the two parameters of the model, viz.,

$$K = \mu_t/\mu_l \tag{12}$$

and

$$G = \langle\tau^3\rangle\langle\tau\rangle/\langle\tau^2\rangle^2 , \tag{13}$$

where μ_t and μ_l are the carrier mobilities perpendicular and parallel to a valley symmetry axis, τ is the carrier scattering probability, and ⟨ ⟩ indicates a weighted average defined by

$$\langle\tau^s\rangle = \frac{\int_0^\infty \tau^s(\partial f_0/\partial E)E^{3/2}dE}{\int_0^\infty (\partial f_0/\partial E)E^{3/2}dE} , \tag{14}$$

where f_0 is the unperturbed Fermi distribution function and E is the carrier energy. The symmetry condition, Eq. (11), holds for all values of K and G.

For the ⟨111⟩-oriented valleys appropriate for PbTe,

$$b = -c = G\left[\frac{(2K+1)^2}{3K(K+2)}\right] - 1 \tag{15}$$

and

$$d = G\left[\frac{2(2K+1)(K-1)^2}{3K(K+2)^2}\right] . \tag{16}$$

If the experimental values of b, c, and d are not exactly consistent with Eq. (11), then the parameter values obtained by solving Eqs. (15) and (16) will depend on which pair of measured values is used to solve for them;[40] in this case, a least-squares fit of all of the data should be applied. However, small inconsistencies may generate insignificant differences. For example, if values of b and d lead to $K = 4$ and $G = 1.10$, then the use of c and d, with $c = -1.02b$, changes K and G by $\frac{1}{2}\%$ or less.

All of the previously published 3C WFMR measurements on bulk samples of PbTe known to me are summarized in Table I.[13–17,41,42] I want to examine these earlier results in some detail, in order to establish as clearly as possible a standard of quality with which to compare the present 4C film data. Unfortunately, this bulk standard must be based mostly on inference and extension, since almost all of the 3C WFMR measurements on bulk crystals were carried out on *p*-type samples, and no complete measurements below 77 K have ever been published for either *n*- or *p*-type bulk PbTe! As far as I know, the paucity of *n*-type data is a historical accident rather than evidence of some basic impediment to obtaining good WFMR data on *n*-type samples. The lack of helium-temperature measurements, on the other hand, clearly reflects the difficulty in obtaining reliable results from very small signals: To remain in the weak-field region, $\Delta\rho \lesssim 0.1\rho_0$ and ρ_0 drops to its smallest value at the lowest temperature, since the highest carrier mobilities occur there *and* no freezeout occurs in undoped PbTe.[12,43]

I examine first the data on *p*-type crystals. All of the measured WFMR coefficients conform closely to the symmetry condition ($x=0$) for the $\langle 111 \rangle$ multivalley model: The average of 13 values of x is $+0.006$.[44] Table I also includes the parameter values obtained by fitting this model to the published WFMR coefficients.[45] Gupta's results indicate that the mobility anisotropy parameter K decreases with increasing carrier density, and almost all of the tabulated values suggest that K decreases with decreasing temperature (between 300 and 77 K). The K values lie in the range 2.5—5.0,[46] considerably less than the valley *mass* anisotropy of about 10 or more.[47,48] In terms of the transport model, this difference is due to the scattering anisotropy factor which is included in the mobility anisotropy K. The temperature dependence of K has been analyzed using a combination of anisotropic optical and isotropic acoustical lattice scattering.[49] The same ingredients do not account for its carrier-concentration dependence.[42]

The definition of the scattering parameter G imposes rather strong constraints on the range of values expected for any reasonable dependence of τ on carrier energy: For classical statistics, G should exceed unity by no more than a few tenths, and should decrease towards unity as the temperature decreases and the statistics become more and more degenerate. The tabulated G values for *p*-type bulk PbTe are therefore very satisfying and help to generate considerable confidence in the validity of the model and in the quality of the samples and experimental techniques.

The last four lines of Table I contain the only 3C WFMR measurements ever published for *n*-type PbTe. The first two of those lines present the data as originally published in 1960.[16] The model-parameter values shown there were derived from averages of WFMR measurements on two samples with essentially identical carrier densities. However, the dimensionless coefficients for *both* samples were calculated using the mobility values given in the table, even though one sample had 300- and

TABLE I. Published three-coefficient WFMR and $\langle 111 \rangle$ multivalley model parameters in cubic PbTe.

First author	Year	Carrier type and density (cm^{-3})	Temperature (K)	Carrier mobility ($cm^2/V\,sec$)	Hall angle tangent $\mu_H B/C$	Dimensionless WFMR coefficients b	c	d	Multivalley model parameters K	G	x
Shogenji[a]	1957	p, 2.5×10^{18}	90	12 800	1.03[b]	0.12	−0.13	0.25	2.96	1.03	−0.040
Shogenji[c]	1959	p, 2.5×10^{18}	90	12 800	0[d]	0.142	−0.145	0.297	3.27	1.04	−0.010
Allgaier[e]	1960	p, 3.5×10^{18}	300	888	0.13	0.345	−0.330	0.520	4.74	1.17	0.029
			77	15 500	0.27	0.151	−0.152	0.394	4.20	1.02	−0.003
Brettell[f]	1968	p, 2×10^{18}	77	5 270	0.29	0.262	−0.258	0.712	7.72	1.05	0.006
Gupta[g]	1977	p, 7.1×10^{17}	300	849	0[d]	0.430	−0.421	0.596	5.02	1.24	0.015
			77	23 100	0	0.227	−0.225	0.552	5.50	1.05	0.004
		p, 2.0×10^{18}	300	872	0	0.355	−0.345	0.512	4.51	1.19	0.020
			77	19 800	0	0.179	−0.180	0.418	4.24	1.04	0.002
		p, 7.0×10^{18}	300	910	0	0.301	−0.294	0.402	3.75	1.17	0.017
			77	10 500	0	0.131	−0.129	0.247	2.91	1.04	0.010
		p, 1.3×10^{19}	300	898	0	0.258	−0.251	0.338	3.36	1.14	0.021
			77	7 020	0	0.110	−0.109	0.186	2.51	1.04	0.005
Allgaier[h]	1960	n, 9.2×10^{17}	300	1670	0.22	0.175	−0.179	0.320	3.35	1.07	0.013
			77	32 700	0.20	0.097	−0.109	0.203	2.51	1.03	−0.059
			300	1 440[i]	0.19	0.234	−0.241	0.432	4.09	1.10	0.013
			77	29 200[i]	0.18	0.127	−0.130	0.247	2.87	1.04	−0.059

[a]Reference 13.
[b]Not in weak-field region, but coefficients and parameters only slightly different from results on same sample, following line.
[c]Reference 15.
[d]Extrapolation to zero magnetic field.
[e]Reference 17.
[f]Reference 41. This sample is actually $Pb_{0.975}Cd_{0.025}Te$.
[g]Reference 42. Data from two WFMR configurations and one "planar Hall coefficient" measurement.
[h]Reference 16.
[i]Results from previous two lines recalculated using these adjusted mobilities. See Sec. II.

77-K carrier mobilities 11% and 14% lower than those values. The justification was that the higher mobility values were normal *and* that this adjustment brought the corresponding WFMR coefficients for the two samples into close agreement with each other.

Because of the central importance of these n-type results to the present measurements, I reexamined the original data to find out what changes would occur if K and G were derived from WFMR coefficients calculated by assuming the *lower* mobility values for both samples. The last two lines in Table I present the results, revealing significant increases in K at both temperatures and corresponding, but much smaller, increases in G. Fortunately, however, the following comments apply to either set of results: The K values are somewhat lower than most of those found in p-type PbTe, but the change in K with temperature, and the magnitudes and temperature trend of G, mirror those found in p-type material.

For the sake of completeness and some additional perspective, I have also analyzed all of the published incomplete 2C WFMR data known to me.[14,50–52] The results are presented in Table II. All of the data were obtained on bulk n- and p-type samples, except for the last two entries. Even though incomplete, values of K and G may be obtained from these data, since the applicability of the $\langle 111 \rangle$ multivalley transport model is firmly established from the analysis of the 3C WFMR measurements. The characteristics of the model parameters summarized in Table II are very different from those in Table I. There is a great deal of scatter in both K and G, including some values which are unrealistic or not allowed ($G < 1$). Part of this scatter resulted from the need to estimate coefficients from published graphical data, but it still appears to me that, as a whole, the quality of samples or measurements is distinctly lower than that associated with the 3C data of Table I.

The last two entries of Table II present 2C WFMR data obtained on films.[51,52] Since the samples may well have been strained, the calculated values of K and G have little or no significance other than to suggest that the data is not reliable. The last entry is so peculiar and atypical ($b \gg d$) that it seems possible that the longitudinal and transverse designations were interchanged on the published figure. Assuming this error was made leads to the K and G values shown in parentheses; the improvement, if any, is minimal.

III. WFMR IN NONCUBIC PbTe

In the Introduction, the 4C WFMR technique was described as a convenient, reliable, and sensitive means of detecting symmetry-lowering effects in oriented films and layers. The possibility of confirming this description provides the main justification for gathering, analyzing, and publishing such a large body of this new kind of WFMR data. I also cited preliminary measurements on PbTe which tend to support the above characterization.[8,9] Actually the expectation of sensitivity originated with our earlier analysis[53] of published WFMR measurements on two sets of (100)-oriented SnTe films, with sample currents parallel to the [100] and [110] directions.[54] We had noticed that the 2C measurements from the first set deviated substantially from those predicted from the values of b, c, and d derived from the 3C second set, and we found that these inconsistencies could be accounted for in terms of a four-coefficient WFMR model with substrate-induced tetragonal symmetry. But the analysis

TABLE II. Published two-coefficient WFMR and $\langle 111 \rangle$ multivalley model parameters in cubic PbTe.

First author	Year	Carrier type and density (cm^{-3})	Temperature (K)	Carrier mobility ($cm^2/V\,sec$)	Hall angle tangent $\mu_H B/C$	Dimensionless WFMR coefficients[a] $b\ (=-c)$	d	Multivalley model parameters K	G
Allgaier[b]	1958	p, 2.4×10^{18}	300	686	0.01	0.60	1.00	9.39	1.31
			77	16 200	0.1	0.32	0.44	4.00	1.17
		p, 3.0×10^{18}	77	14 600	0.2	0.21	0.48	4.75	1.06
Putley[c]	1955	n, 5.8×10^{15}	290	1 200	0.13	0.56	0.56	4.29	1.38
			77	14 800	0.09	1.27	1.63	13.4	1.82
			20	102 000	0.20	1.60	1.94	15.2	2.07
Allgaier[b]	1958	n, 5.8×10^{17}	77	27 700	0.4	0.12	0.25	2.96	1.03
		n, 9.5×10^{18}	77	10 700	0.1	0.13	0.60	6.95	.95
		n, 9.5×10^{18}	77	10 700	0.38	0.14	0.47	4.95	.99
Makino[d,e]	1964	n, 2.5×10^{17}	4.2	30 000	0.1	0.39	0.63	5.56	1.19
Zemel[e,f]	1965	g	77	g	0.18	0.56	0.14	1.92	1.53
						(0.14)[h]	(0.56)	(6.18)[h]	(0.97)

[a]Determined from experimental data by assuming $c = -b$.
[b]Reference 14.
[c]Reference 50.
[d]Reference 51.
[e]Thin-film sample.
[f]Reference 52.
[g]Data not given in paper.
[h]Values of K and G obtained by interchanging b and d values from the previous line. See Sec. II.

of data from *different* samples requires the assumption that they have identical characteristics, a circumstance which does not support claims of convenience or reliability.

The key to achieving these last two characteristics lies in the ability to measure four potentially independent WFMR coefficients on one sample. We realized earlier that this can be done whenever WFMR "skewness" is present.[4–6] We have used this term to describe a rotational sinusoidal WFMR pattern in a plane for which the extrema occur in nonspecial configurations determined by the values of the coefficients, not by crystallographic constraints. The maximum, minimum, and phase of this general sine curve allow three combinations of WFMR coefficients to be measured, and a fourth is easily obtained by orienting $\vec{B}$ normal to the plane in which the skewed curve was generated. Convenience is truly achieved via this 4C, single-sample WFMR technique because detecting skewness does *not* require rotating $\vec{B}$ in some experimentally awkward, obliquely oriented plane. It is generally present in planes of rotation perpendicular to the (111) plane, as will be outlined below. It is even present in the high-symmetry (100) plane, as long as the sample current is *not* parallel to the [100] or [110] directions—the two that are always used when taking WFMR data in this plane![6]

I briefly outline the 4C generalization of the SPS WFMR phenomenology, Eq. (2), as it was developed for the present case of a (111)-oriented film, with the assumption that strain will produce a uniform trigonal distortion, with the trigonal axis normal to the film plane.[4,5] Equation (1) still holds, with the understanding that μ_H now refers to the component of the Hall mobility (measured or calculated) obtained with $\vec{B}$ normal to the film plane. The first step is to transform Eq. (2) to the sample-oriented coordinate system defined in Fig. 1. Note that this figure also identifies an alternative, equally convenient set of rotated coordinate axes which, when dealing with WFMR, is *not* equivalent to the chosen set. The chosen axes [1], [2], and [3] correspond to the binary, bisectrix, and trigonal axes in a trigonal crystal such as bismuth.

At the crystallographic level, there are eight independent WFMR coefficients when trigonal symmetry applies.[1] But with the present restriction of the sample current to directions lying *in* the (111) plane, only four coefficients are measurable. This is just sufficient to determine that one of them is related to the other three, as must be the case when the three-coefficient cubically symmetric SPS phenomenology applies. Even with this sample-current constraint, however, the generalization of Eq. (2) remains too cumbersome to be useful. Our earlier analysis therefore compromised by developing 4C generalizations for rotations of $\vec{B}$ in the three mutually perpendicular and experimentally convenient planes defined in Fig. 2. They are (*A*) the film plane itself, (*B*) the plane perpendicular to the film *and* to the sample current, and (*C*) the plane perpendicular to the film which contains the sample current.

The 4C WFMR generalizations in these planes are

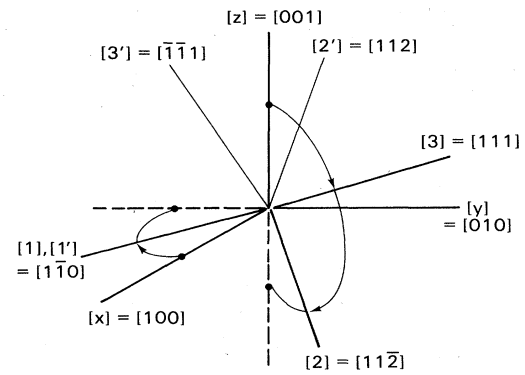

FIG. 1. Sample-oriented coordinate axes [1], [2], [3] used for WFMR data and analysis, and an unused alternative [1'], [2'], [3'], relative to the cubic axes [x], [y], and [z].

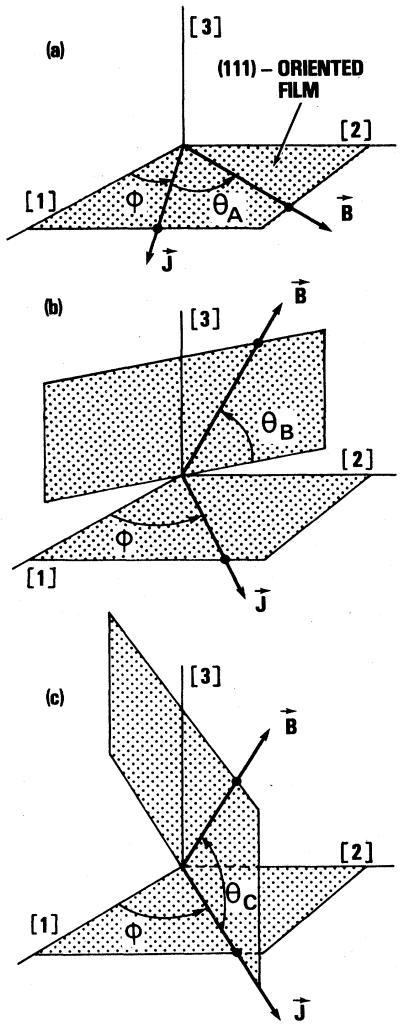

FIG. 2. Planar configurations used for rotational WFMR: (a), in plane; (b) all transverse; (c), transverse longitudinal. ϕ and $\theta_{A,B,C}$ specify the directions of current density $\vec{J}$ and magnetic field $\vec{B}$. Sample-oriented coordinate axes [1], [2], and [3] are defined in Fig. 1.

$$M_{\phi}^{\theta_A}=b+\tfrac{1}{2}c+\tfrac{1}{3}d+(\tfrac{1}{2}c+\tfrac{1}{6}d)\cos(2\theta_A)\ , \tag{17}$$

$$M_{\phi}^{\theta_B}=b+\tfrac{1}{4}d-\tfrac{1}{12}d\cos(2\theta_B)+\tfrac{1}{6}\sqrt{2}d'\cos(3\phi)\sin(2\theta_B)\ , \tag{18}$$

and

$$M_{\phi}^{\theta_C}=b+\tfrac{1}{2}c+\tfrac{5}{12}d+(\tfrac{1}{2}c+\tfrac{1}{12}d)\cos(2\theta_C)+\tfrac{1}{6}\sqrt{2}d'\sin(3\phi)\sin(2\theta_C)\ , \tag{19}$$

where b, c, d, and d' are the generalized SPS coefficients, and Fig. 2 defines ϕ and $\theta_{A,B,\text{ or }C}$, the sample-current and magnetic-field directions. These equations demonstrate that in planar configuration A there is no skewness and the WFMR does not depend on ϕ. Skewness does occur in planar configurations B and C, due to the presence of the term containing d' in each of those configurations. It is ϕ dependent and vanishes every 120°, but not at the same ϕ in both configurations; therefore no current direction exists which will prevent the determination of all four WFMR coefficients from measurements in planar configuration A and in one of the other two. The presence of just four WFMR coefficients in Eqs. (17)—(19) is due to the presence of two constraints on the six constants needed to describe two independent general sine curves: No skewness is allowed in configuration A, and plane A intersects planes B and C.

The four generalized WFMR coefficients were defined so that for cubic symmetry, $d'=d$, and b, c, and d reduce to their original definitions in that case. Equations (17)—(19) also encompass a third class of crystallographic symmetry, hexagonal; in this case, $d'=0$, with no constraints on d or the other coefficients. Note that a strained cubic crystal may not become *crystallographically* hexagonal, but as will be seen below, a strain-induced simplification of the band structure can lead to an electronically hexagonal transport environment. Note also that skewness vanishes in the hexagonal case (for all ϕ), but not for cubic symmetry. Since skewness is very ϕ sensitive, a glance at WFMR data in configurations B and C does *not* necessarily make it obvious that the crystal is strained.

It will sometimes be convenient to discuss some of the present experimental data in terms of the WFMR in three *standard* configurations, viz., when $\vec{B}$ is parallel to the sample current, and when it is perpendicular to the sample current and in the film plane or perpendicular to it. According to Eqs. (17)—(19), none of these three configurations involves d', and therefore they do not depend on the choice of current direction ϕ. Thus for the case $\phi=0$, these three configurations become M_1, M_1^2, and M_1^3, respectively, where the subscripts and superscripts refer to the axes of the sample-oriented coordinate system of Fig. 2. This nomenclature is useful because it emphasizes the fact that $\vec{B}$ is oriented in three mutually perpendicular directions in the three standard configurations. Using Eqs. (17) and (18) or (19) leads to

$$M_1=b+c+\tfrac{1}{2}d\ , \tag{20}$$

$$M_1^2=b+\tfrac{1}{6}d\ , \tag{21}$$

and

$$M_1^3=b+\tfrac{1}{3}d\ . \tag{22}$$

These three WFMR coefficients *look* the same as those given in Eqs. (8)—(10) for the cubic case. We have repeated them here, with the new M_{ϕ}^{θ} notation, to emphasize that they *correspond* to Eqs. (8)—(10), but are identical to them only if the crystal turns out to be cubic. The distinction is simply that the coefficients b, c, and d have a more general meaning in Eqs. (17)—(19) than in the cubic case.

As far as I know, the only published papers on experimental 4C WFMR measurements are the two containing our earlier data on (111)-oriented n-type PbTe films. Those results include a single room-temperature run on a sample grown by Lopez-Otero, runs at 300 and 77 K on a film prepared at our laboratory,[8] and a series of room-temperature runs on two other Lopez-Otero samples, carried out in the course of a study on the effect of thermal cycling on room-temperature strain.[9] Those earlier 4C WFMR measurements were found to conform to the general behavior predicted by Eqs. (17)—(19). The correspondence was especially close in the second paper.[55] The WFMR coefficients obtained by least-squares fitting Eqs. (17)—(19) to the measurements from the three runs on the first pair of samples, and from four selected runs on the second pair, are summarized in Table III. The results reveal that $d'<d$ in every case, substantially less in most cases. When published in 1980, the room-temperature results provided the first evidence that PbTe films deposited on BaF_2 were under a detectable amount of strain at that temperature. The four runs selected from the thermal cycling study are initial-final pairs. In each case, the d'/d ratio after the thermal cycling was found to be closer to unity than before, suggesting that most of the strain at 300 K had been relieved by repeated cycling between 300 and 4.2 K.

To extract further information from the previously published 4C WFMR coefficients summarized in Table III, it was necessary to move from the crystallographic to the electronic level, i.e., to select and apply a transport model to the analysis of the data. In those earlier papers, we used the simplest imaginable generalization of the cubic $\langle 111\rangle$ multivalley model, assuming that the only effect of a trigonal distortion was an intervalley carrier transfer resulting from the removal of the valley band-edge energy degeneracy. Clearly, the changes in valley orientations due to strain are negligible, but it is less justifiable to assume that the same K and G values can characterize transport in all four valleys, especially when their carrier densities become substantially different. It is clear, for example, that G must depend on carrier density for the general case of Fermi-Dirac statistics.

Thus the simple trigonal model requires only one additional parameter, a carrier transfer factor

$$F=n_1/n_3\ , \tag{23}$$

TABLE III. Previously published four-coefficient WFMR and trigonal model parameters in (111)-oriented *n*-type PbTe films.

Temperature (K), run number	Carrier density (10^{16} cm^{-3})	Carrier mobility (cm^2/V sec)	Hall angle tangent $\mu_H B/C$	Dimensionless WFMR coefficients b	c	d	d'	Trigonal model parameters[a] and fitting error F	K	G	z[b]	E[c] (10^{-2})
(A) Sample L1513, d (thickness)=4.0 μm												
300A	10	1560	0.16	−0.070	−0.602	1.66	0.244	3.98	10.2	1.23	0.65	1.8
(B) Sample 79-38, d=10.4 μm												
300A	3.7	1360	0.10	0.129	−0.481	1.17	0.823	1.50	28.3	1.05	0.28	10
77A	3.3	34,900	0.14	0.042	−0.196	0.464	0.349	2.34	7.88	0.97	0.22	14
(C) Sample P04, d=24.5 μm												
300A	4.3	1450	0.10	0.190	−0.248	0.525	0.416	1.18	4.53	1.08	0.49	0.4
300D	4.5	1430	0.10	0.224	−0.217	0.434	0.413	1.01	4.14	1.08	0.54	2.1
(D) Sample P07, d=15.5 μm												
300A	8.3	1560	0.11	0.180	−0.203	0.411	0.333	1.13	3.71	1.07	0.55	2.1
300Y	8.9	1510	0.11	0.203	−0.202	0.388	0.344	1.04	3.67	1.08	0.57	3.0

[a]See Sec. III and Appendix A.

[b]z is the measured WFMR symmetry $(b+c+\frac{1}{2}d)/d'$, which equals $\frac{1}{2}$ for the trigonal model.

[c]E is the rms fractional deviation between the four measured and calculated WFMR coefficients.

where n_1 and n_3 are the carrier densities in the single valley normal to the film plane and in *each* of the other three. The expressions derived for b, c, d, and d' in this simple three-parameter (F-K-G) model are surprisingly long and cumbersome and are summarized in Appendix A. What remains simple and compact is the symmetry condition which relates the four WFMR coefficients, viz.,

$$b+c=\tfrac{1}{2}(d'-d)\ . \tag{24}$$

This reduces, as it must, to the condition for the cubic case, $b+c=0$ for $d'=d$. When the sample is only very slightly strained, both sides of Eq. (24) become very small. A more reasonable test of the applicability of the F-K-G model is then obtained from a rearrangement of this equation,

$$M_1=b+c+\tfrac{1}{2}d=\tfrac{1}{2}d'\ , \tag{25}$$

where, as noted earlier, M_1 actually represents the longitudinal WFMR for *any* current direction ϕ. As a convenient means of assessing the conformity of the present WFMR measurements to the predictions of the F-K-G model, I will define two symmetry parameters, based on Eqs. (24) and (25),

$$y=(b+c)/(d'-d) \tag{26}$$

and

$$z=M_1/d'\ . \tag{27}$$

Both parameters equal $\frac{1}{2}$ when the model fits perfectly.

The F-K-G model predicts that both sides of Eq. (24) become negative ($d'<d$) when $F>1$. As noted in the Introduction, this transfer of carriers into the single valley normal to the film plane corresponds to an antibismuth trigonal distortion, i.e., to an in-plane stretching of the film. It has been known for many years that this kind of strain lowers the single-valley band-edge energy relative to the other three (in both conduction and valence bands, actually). This has been predicted theoretically,[23] but even earlier was deduced from the signs of the measured piezoresistance coefficients in n- and p-type PbTe.[56] Note that a complete transfer of carriers into the single valley ($F=\infty$) makes $d'=0$ (see Appendix A), the condition for hexagonal symmetry. This is to be expected, since the rotational symmetry of a single valley is effectively hexagonal.

Least-squares fits of the sets of four WFMR coefficients summarized in Table III to the F-K-G model are included in the table. Also shown are values of the symmetry parameter z as well as another important "quality index" of the model, E, the root-mean-square fractional difference between the experimental and calculated values of the four coefficients. The fitted values of F are all greater than one; F is largest in the thinnest sample (L-1513), it increases with decreasing temperature in sample 79-38, corresponding to an increasing strain (something that was not obvious from the values of d' and d at 300 and 77 K), and its value after the thermal cycling of samples P04 and P07 suggests more quantitatively that the cycling process has eliminated most, if not all, of their room-temperature strains. However, the large F value in sample L-1513 must be viewed in the light of what will turn out to be uncharacteristically high K and G values for room-temperature WFMR data.

The K values for sample 79-38 are definitely unreasonable, the G value at 77 K is outside the range permitted by its definition, and the magnitudes of the symmetry and error parameters suggest that there is possibly a problem with this sample. The analysis of the present WFMR measurements at 300 and 77 K will establish that the model is not at fault. The situation began to improve with thermally cycled samples P04 and P07. Note that the K values for these two films are not very different from those summarized in Table I for bulk samples, and the G values from the cycled films and the bulk crystals are essentially indistinguishable.

These last results, quite typical of those obtained during the course of the thermal-cycling study, provided the stimulus for embarking on the much more extensive series of 4C WFMR measurements (including the most difficult case of measurements at 4.2 K) which ultimately led to the results presented in Sec. V of this paper.

IV. EXPERIMENTAL DETAILS

The measurements reported in this paper were carried out on PbTe films epitaxially deposited on cleaved (111)-oriented faces of BaF_2 using the hot-wall technique.[10] Source and substrate temperatures, deposition rates, film thicknesses, and current orientations are summarized in Table IV for the four samples studied. Hall bar profiles were photolithographically prepared. The shapes for the first three and the last samples in Table IV were similar to those shown in parts (a) and (b) in Fig. 1 from Ref. 27. Gold films were deposited on the end and side contacts of the samples, and gold-wire leads were attached to them by thermal compression bonding.

All measurements were carried out in a Janis Super Vari-Temp Dewar. Sample currents of 10 mA or less were provided by a Keithley regulated-current supply. A Harvey Wells electromagnet was used for the Hall and magnetoresistance measurements. The magnetic field intensity was determined from a calibrated Hall probe. Voltages for all measured quantities, appropriately sequenced, were obtained from a Hewlett-Packard scanner and a $6\frac{1}{2}$-place digital voltmeter. Data acquisition, processing, storage, and display were controlled and executed by a PDP model no. 11/40 computer system.

At the beginning of each run, Hall mobilities were determined from conventional measurements of the weak-field Hall coefficient and zero-field resistivity, so that the *dimensionless* WFMR coefficients [see Eq. (1)] could be calculated as soon as the necessary WFMR measurements were carried out. A run consisted of rotations of $\vec{B}$ in two planar configurations, A (in plane) and B (all transverse) *or* A and C (transverse longitudinal) as described in Fig. 2. During the course of each rotation through 400° (a 40° overlap served to check for drifts or other undesirable events), WFMR data at an appropriate fixed magnitude of $\vec{B}$ were taken at 10° intervals. Generally, each data point was an average of three sets of the

TABLE IV. Sample parameters.

Sample number	Sample source	Current orientation ϕ[a]	Source temperature (°C)	Substrate temperature (°C)	Growth rate $\mu m/h$	Film thickness (μm)
P07	Linz	−20°	≈550	≈450	5–10	15.5
P15	Linz	99°	≈550	≈450	5–10	11.3
P16	Linz	99°	≈550	≈450	5–10	11.3
P22	NSWC	−90°	550	340	8.5	4.3

[a]The current direction ϕ is defined in Fig. 2.

usual four combinations of forward and reverse sample-current and magnetic-field directions. To obtain $\Delta\rho/\rho_0$, these WFMR measurements were compared with values of the zero-field resistivity determined at the beginning, midpoint, and conclusion of each planar rotation. Since each run consisted of about 10^3 individual measurements, it was the use of a modern computer that made it practical and convenient to carry out and analyze the large number of runs reported in this paper. Before 1960, when it was common to take data the old-fashioned way—by hand—it would require a day or two to complete a single two-rotation run (usually involving a much smaller total number of individual measurements). Each complete run reported in this paper was carried out in about one half-hour.

For each of the 48 runs, the 82 data ponts which comprised a run were least-squares fit to the appropriate pair from Eqs. (17)–(19). Of course, ideally, the four WFMR coefficients of the generalized SPS phenomenology could have been determined from just four, not 82, appropriately chosen data points. For example, measurements in the three standard configurations, Eqs. (20)–(22), plus a fourth with $\vec{B}$ in some oblique orientation from planar configuration B or C, would have sufficed. But these very highly overdetermined data sets established that the measurements actually correspond to WFMR (sinusoidal) behavior, and conform to the constraints imposed by trigonal crystallographic symmetry (which of course includes cubic and hexagonal as special cases). Moreover, they made it possible to obtain much more accurate values of the four coefficients, especially d', which (as will be seen in the next section) became small at low temperatures in three of the samples investigated.

The second procedure which was applied to all 48 WFMR runs was a least-squares fit of the four coefficients to the F-K-G model. Alternative models were also applied to the WFMR data from some runs, as appropriate.

V. RESULTS AND DISCUSSION

A. General remarks

The results presented in this paper include 48 complete runs on four samples from two sources. The measured dimensionless WFMR data from selected runs are plotted in Figs. 3–6. The solid lines in each figure are the least-squares fit to the generalized SPS WFMR phenomenolo-

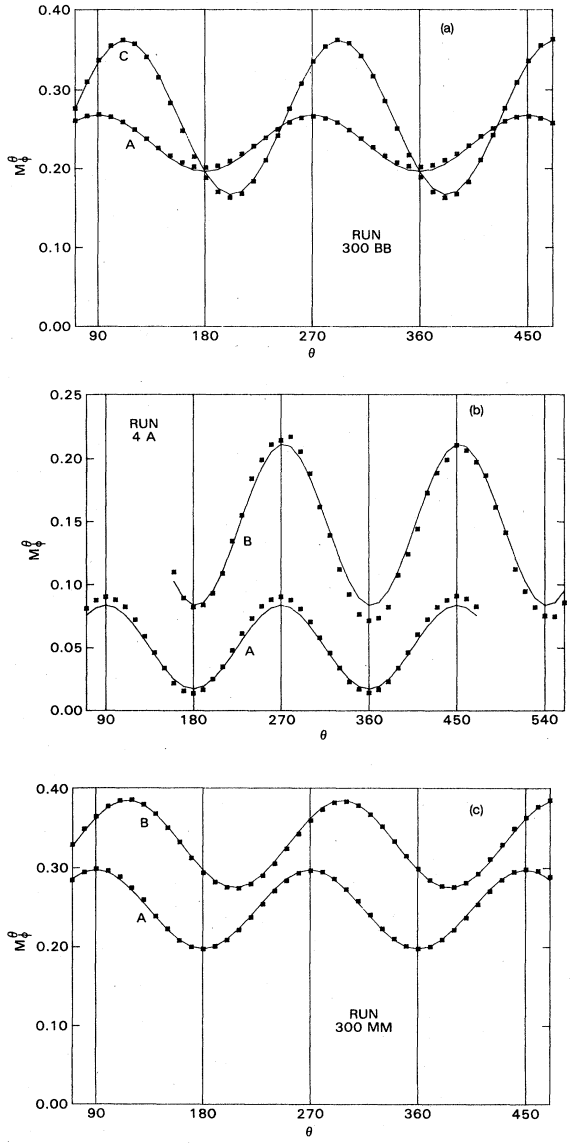

FIG. 3. Measured WFMR M_ϕ^θ versus magnetic field direction θ for sample P07: (a) run 300BB, (b) run 4A, (c) run 300MM. Dimensionless coefficients M_ϕ^θ are defined by Eq. (1) and by Figs. 1 and 2. Planar configurations A and B or C (see Fig. 2) used for each run are indicated on the figures. The squares are the experimental results, and the solid straight-line segments connect a set of calculated points for the same θ values which are the least-squares fit to the experimental data.

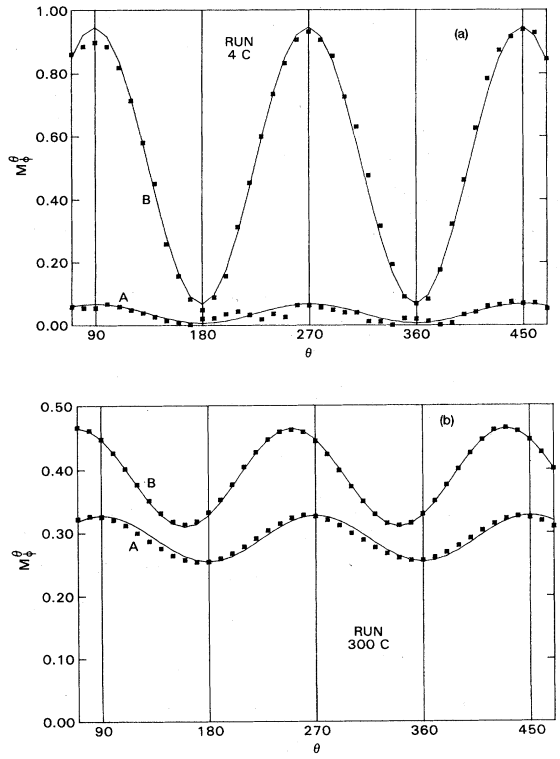

FIG. 4. Measured WFMR M_ϕ^θ versus magnetic field direction θ for sample P15: (a) run 4C, (b) run 300C. See Fig. 3 caption for further details.

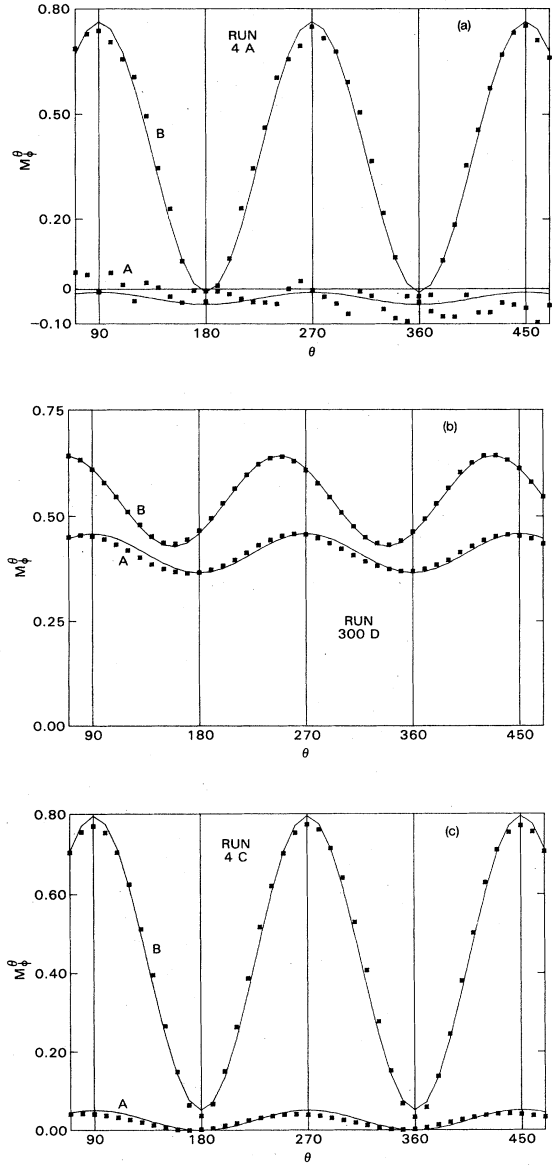

FIG. 5. Measured WFMR M_ϕ^θ versus magnetic field direction θ for sample P16: (a) run 4A, (b) run 300D, (c) run 4C. See Fig. 3 caption for further details.

gy, Eqs. (17)—(19). Note that those lines are composed of straight-line segments connecting sets of computer-generated points for the same values of $\theta_{A,B,\text{ or }C}$ at which the experimental data were obtained. In the best cases, the fit is so close that the line segments simply appear to connect the experimental points. For balance, I have also included a run [Fig. 5(a)] which was by far the worst of the 48; fortunately, it was unique. Its most glaring fault is a best fit of the very noisy planar configuration-A data which is negative at all values of θ_A.

The numerical results for all 48 runs are presented in Table V *in chronological order.* The table includes the carrier density and mobility, the tangent of the Hall angle for the $|\vec{B}|$ at which each run was carried out, sets of best-fit WFMR coefficients b, c, d, and d' derived from the 82 experimental data points from each run, the best-fit parameter values for the F-K-G model, the 4C WFMR symmetry parameters y or z, and the rms fitting errors E for the model.

The carrier densities in the four samples lie between 6×10^{16} and 1×10^{17} cm^{-3}, with corresponding degeneracy temperatures between about 50 and 70 K. These values would be more than twice as high if the indicated carrier densities were completely contained in a single valley. The carrier mobilities at 300 and 77 K lie in the ranges 1100—1500 and 29 000—38 000 cm^2/V sec, characteristic of good-to-excellent quality bulk material.[12,43] At 4.2 K, the measured mobilities of 250 000—500 000 cm^2/V sec are not nearly as high as some of the values [(1—5)$\times10^6$ cm^2/V sec] that have been reported on both bulk and film samples of PbTe at that temperature.[10,57] But these lower mobilities fare well when compared with those found in most other uniformly doped semiconductors at low temperatures,[58] because the very high dielectric constant in PbTe weakens the effect of ionized impurity scattering.[59]

The overall general characteristics of the tabulated 4C WFMR coefficients may be summarized as follows: With rare exceptions, $b < |c|$ *and* $d' < d$; d'/d decreases with decreasing temperature, becoming very small and even slightly negative at 4.2 K; c is always negative; and b is always positive at 77 and 300 K and always negative at 4.2 K. Bulk WFMR measurements on PbTe have never yielded $b < 0$, nor have they ever achieved the very small

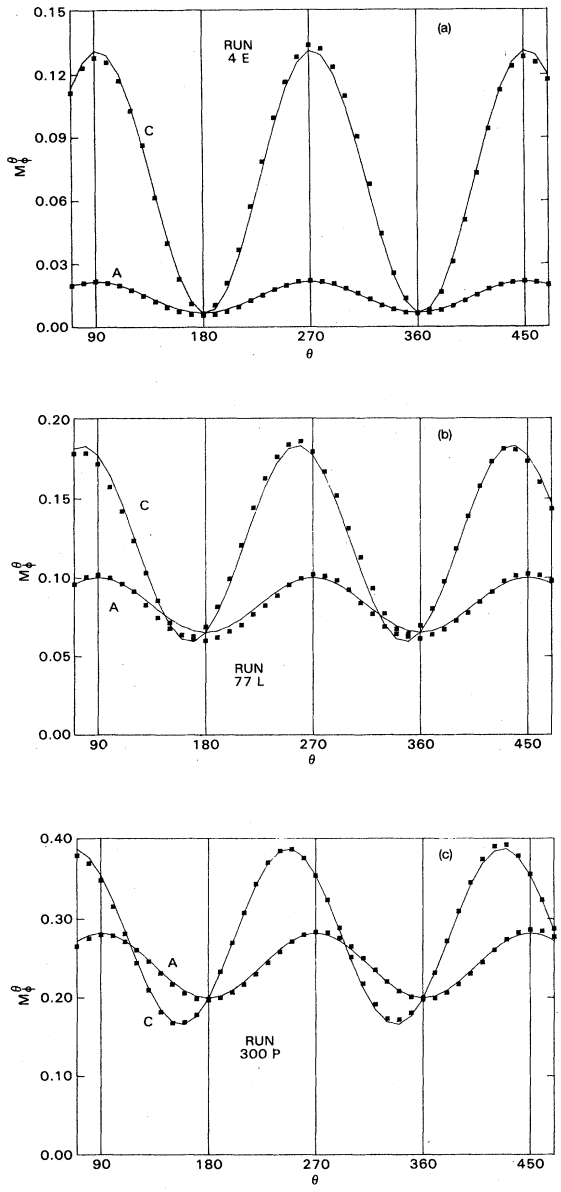

FIG. 6. Measured WFMR M_ϕ^θ versus magnetic field direction θ for sample P22: (a) run $4E$, (b) run $77L$, (c) run $300P$. See Fig. 3 caption for further details.

values of M_ϕ^θ, both longitudinal and transverse, seen in the film measurements in planar configuration A at 4.2 K, Figs. 4(a), 5(c), and 6(a). Note that no discrepancy is implied by the differences between the present results and the older data on bulk samples. The four-coefficient generalization of WFMR is not subject to the constraints imposed on the three-coefficient SPS formulation by the requirements of cubic symmetry. As will be discussed in Secs. V C and V D, these differences immediately establish that the WFMR is a very sensitive detector of symmetry-lowering effects in a multivalley semiconductor.

B. WFMR behavior and the *F-K-G* model

In this section, I will take a more detailed look at the WFMR behavior found in the 48 runs. I discuss the results sample by sample, since each sample has its own run history and exhibits certain characteristics which distinguish it from the others. It is very useful to relate most of this discussion to the fitted parameters of the *F-K-G* model. Although there may be some questions about the validity of this model, especially at 4.2 K, the model fits the measured WFMR coefficients very well in almost every run, with rms errors of the order of 10^{-2}. In any case, it is much easier to characterize and evaluate WFMR behavior in terms of F, K, and G than in terms of

1. Sample P07

This sample is one of the two which had been used in the earlier thermal-cycling study.[9] The parameters of the *F-K-G* model on the first line of Table V (which are very close to those on the last line of the summary of earlier 4C WFMR measurements, Table III) suggest that at the beginning of the present study there was not much strain left in this sample at 300 K. A long series of runs at 300 K were then carried out (to check for long-term drifts and run-to-run scatter), followed by single runs at 4.2 and 77 K, and then by three final runs at 300 K.

The model parameters at 300 K are quite close to those from the meager supply of WFMR data on n-type bulk PbTe, Table I. There is some run-to-run noise in the room-temperature parameters, with F and G being the most and the least sensitive to the imperfectly controlled and executed measurement process. The successive runs $300GG$ and HH yielded the largest and smallest F values from any of the room-temperature runs, and they are probably not entirely due to random noise. They immediately followed a switch from using planar configurations A and C to A and B. This required a reorientation of the sample platform which involved flexing of the sample leads. One more thermal cycle seems to have benefited the three final 300-K runs ($300LL$-NN): They are exceptionally consistent, and as a group suggest the closest approach [F(average)$=1.003$] of this (or any other) sample to a strain-free condition at room temperature.

The results of the 77-K run on sample P07 are a great improvement over the only previous (and rather peculiar) 4C WFMR measurements taken at 77 K, line 3 of Table III. The model fit of the newer result corresponds to a modest increase in F (1.27), an essentially unchanged K, and a G which is 4% lower, relative to their values at 300 K. The temperature dependence of G is very typical of the behavior found in bulk crystals, but that of K is not. The latter observation might be a reflection of a lower carrier density, since Gupta's lowest carrier-concentration sample of bulk p-type PbTe yielded a K which actually increases with decreasing temperature.[42]

The run at 4.2 K represents the first *complete* set of WFMR data—3C or 4C—ever reported for n- or p-type PbTe, in bulk or thin-film form, at any temperature below 77 K. Its characteristics correspond to the largest transfer

TABLE V. Measured four-coefficient WFMR and best-fit trigonal model parameters in (111)-oriented *n*-type PbTe films.

Temperature (K), run number	Carrier density (10^{16} cm^{-3})	Carrier mobility (cm^2/V sec)	Hall angle tangent $\mu_H B/C$	Dimensionless WFMR coefficients b	c	d	d'	Trigonal model parameters and fitting error F	K	G	$z,(y)$[a]	E[b] (10^{-2})
(a) Sample P07, d (thickness) = 15.5 μm (see Table III for earlier measurements)												
300*BB*	8.9	1520	0.11	0.202	−0.203	0.394	0.343	1.05	3.68	1.08	0.57	3.2
300*CC*	9.6	1450	0.10	0.213	−0.222	0.428	0.347	1.09	3.76	1.09	0.59	3.9
300*DD*	9.6	1470	0.10	0.211	−0.218	0.424	0.348	1.08	3.76	1.09	0.59	3.8
300*EE*	9.6	1460	0.10	0.210	−0.221	0.433	0.347	1.10	3.78	1.09	0.59	3.9
300*GG*	10.0	1390	0.10	0.206	−0.262	0.521	0.313	1.29	3.73	1.12	0.65	5.2
300*HH*	9.9	1440	0.10	0.235	−0.211	0.353	0.373	0.95	3.67	1.10	0.54	1.6
300*II*	9.8	1420	0.10	0.217	−0.260	0.481	0.402	1.12	4.16	1.10	0.49	0.4
300*JJ*	9.9	1410	0.10	0.210	−0.270	0.504	0.385	1.18	4.14	1.11	0.50	0.1
300*KK*	10.0	1430	0.10	0.212	−0.216	0.409	0.371	1.04	3.84	1.09	0.54	1.8
4*A*	9.9	403 000	0.50	−0.044	−0.322	0.767	0.049	12.7	4.27	1.16	(0.51)	(0.2)
77*A*	8.9	29 400	0.29	0.142	−0.189	0.437	0.309	1.27	3.81	1.05	0.56	2.5
300*LL*	9.9	1420	0.10	0.236	−0.218	0.392	0.387	0.98	3.85	1.09	0.55	2.4
300*MM*	9.8	1440	0.10	0.232	−0.232	0.394	0.384	1.01	3.81	1.10	0.51	0.6
300*NN*	9.9	1430	0.10	0.228	−0.218	0.402	0.368	1.02	3.78	1.09	0.57	3.3
(b) Sample P15, d = 11.3 μm												
4*C*	6.1	242 000	0.30	−0.814	−1.823	5.288	0.066	28.7	32.6	1.89	(0.50)	0.9
300*B*	7.3	1300	0.09	0.207	−0.308	0.722	0.477	1.29	5.67	1.10	0.55	(0.7)
300*C*		1300		0.207	−0.314	0.723	0.451	1.33	5.43	1.11	0.56	(0.9)
300*D*	c	1290	c	0.213	−0.308	0.690	0.499	1.23	5.64	1.10	0.50	(0.1)
300*E*		1290		0.208	−0.313	0.715	0.474	1.29	5.56	1.10	0.53	(0.5)
(c) Sample P16, d = 11.3 μm												
300*A*	7.1	1140	0.08	0.287	−0.412	0.966	0.677	1.21	8.16	1.14	0.53	(0.6)
300*B*	7.1	1150	0.08	0.244	−0.433	1.033	0.601	1.35	7.87	1.15	0.54	(0.8)
4*A*	6.1	307 000	0.39	−0.786	−1.588	4.659	−0.058	1160	45.8	1.80	(0.50)	(3.4)
4*B*	6.1	313 000	0.39	−0.835	−1.854	5.405	−0.121	2330	16.1	1.96	(0.49)	(6.1)
300*C*	7.3	1150	0.08	0.288	−0.390	0.910	0.658	1.19	7.67	1.14	0.54	(0.8)
300*D*	7.3	1130	c	0.303	−0.403	0.929	0.685	1.17	7.92	1.14	0.53	(0.7)
300*E*	7.4	1100		0.313	−0.419	0.947	0.717	1.15	8.25	1.15	0.51	(0.3)
4*C*	6.1	283 000	0.37	−0.696	−1.547	4.486	−0.058	1480	15.9	1.80	(0.49)	(2.9)
4*D*	6.1	283 000	0.51	−0.560	−1.282	3.680	−0.030	1510	12.4	1.67	(0.50)	(1.6)
300*F*	7.3	1100	0.08	0.305	−0.432	0.985	0.717	1.17	8.49	1.15	0.51	0.4
300*G*	c	1090	c	0.305	−0.429	0.989	0.710	1.18	8.49	1.15	0.52	(0.5)
300*H*		1090		0.310	−0.424	0.969	0.714	1.17	8.37	1.15	0.52	(0.4)

TABLE V. (*Continued*).

Temperature (K), run number	Carrier density (10^{16} cm^{-3})	Carrier mobility (cm^2/V sec)	Hall angle tangent $\mu_H B/C$	Dimensionless WFMR coefficients b	c	d	d'	F	Trigonal model parameters and fitting error K	G	$z,(y)$[a]	E[b] (10^{-2})
				(d) Sample P22, $d=4.3$ μm								
300*A*	9.6	1200	0.12	0.325	−0.348	0.654	0.499	1.10	4.93	1.17	0.61	4.3
300*B*	9.6	1190	0.09	0.296	−0.389	0.824	0.488	1.24	5.29	1.18	0.65	5.5
4*C*	7.6	495 000	0.45	−0.092	−0.242	0.680	−0.004	1500	7.24	1.13	(0.49)	(0.3)
4*D*		c	0.45	−0.091	−0.240	0.677	−0.021	2720	7.17	1.13	(0.47)	(1.1)
4*E*		506 000	0.61	−0.088	−0.234	0.658	−0.022	2340	6.98	1.13	(0.49)	(1.2)
4*F*	c	c	0.46	−0.090	−0.240	0.675	−0.030	4000	7.14	1.13	(0.47)	(1.5
4*G*		505 000	0.46	−0.091	−0.241	0.679	−0.030	3640	7.19	1.13	(0.47)	(1.5)
4*H*		473 000	1.42[d]	−0.070	−0.186	0.526	−0.010	2280	7.24	1.10	(0.48)	(0.6)
300*I*	9.8	1470	0.10	0.213	−0.228	0.434	0.357	1.09	3.82	1.10	0.57	2.8
300*J*		c	0.10	0.202	−0.245	0.485	0.346	1.19	3.90	1.10	0.58	3.1
300*K*	c	1450	0.07	0.224	−0.225	0.398	0.356	1.04	3.70	1.10	0.56	2.4
77*L*	7.9	36 700	0.34	0.023	−0.190	0.464	0.114	4.68	4.22	1.06	0.57	1.4
77*M*	c	37 300	0.27	0.023	−0.193	0.477	0.110	4.77	4.11	1.06	0.62	2.1
77*N*		38 100	0.19	0.018	−0.198	0.504	0.119	4.78	4.61	1.06	0.61	2.0
300*P*	9.8	1480	0.15	0.209	−0.229	0.439	0.340	1.13	3.74	1.10	0.59	3.5
300*R*		c	0.11	0.213	−0.231	0.435	0.340	1.12	3.72	1.10	0.59	3.5
300*S*	c	1460	0.08	0.213	−0.226	0.416	0.350	1.08	3.73	1.10	0.56	2.4

[a]The symmetry parameters are determined from the measured values of b, c, d, and d' and are defined by Eqs. (26) and (27). The numbers with and without parentheses refer to y and z, respectively. The rationale for using alternative definitions of WFMR symmetry is explained in Sec. III.

[b]The numbers without parentheses are the rms *fractional* difference between the experimental and calculated best fit coefficients. When parentheses are present, the number is the difference itself. This alternative was used, in most cases, to avoid placing too much weight on very small coefficients (usually d' at 4.2 K) when they appeared.

[c]Missing quantities were not remeasured for those runs.

[d]The weak-field condition was deliberately violated, but the results were analyzed as WFMR.

of carriers into the single valley ($F=12.7$, or about 80%) ever deduced from WFMR measurements, yielded a d'/d ratio which has dropped to only 0.06, and provide the first observation of a negative b value. Another distinguishing feature of the results of this run at 4.2 K is the increase in K and G, relative to their values at 77 *and* 300 K. Precisely what is to be expected from these parameters at 4.2 K is not clear, due to the complete change from essentially pure lattice to pure defect scattering. However, this sample is so degenerate at helium temperatures that no reasonable energy dependence of scattering time τ should ever lead to a G value which differs from unity by more than 1 or 2%. This unusual behavior of G at 4.2 K was also found in the remaining three samples, and will be discussed in Sec. V C.

More positive comments about this first 4.2 K run may be made concerning the closeness of the symmetry parameter y to the expected value of $\frac{1}{2}$, reinforced by the very small rms error, 2×10^{-3}. Note that with this run, we switched from z to y and from a least-squares fit based on minimizing the rms *fractional difference* to one based on the rms *difference* itself. The symmetry parameter z in this case is too demanding a test of WFMR symmetry ($z=0.36$ for this run), since it compares two quantities which have become quite small. Also, the *fractional* error has become less appropriate for these results, since it places too much weight on fitting the small coefficient d'.

2. Sample P15

This sample, unlike P07, had not been subjected to extensive thermal cycling between 300 and 4.2 K. Consequently, it is not surprising to find a larger F, 1.29, for the average of the four room-temperature runs, actually slightly larger than that found in sample P07 at 77 K. The G values are practically identical to those found in P07 at 300 K, but K has increased significantly to about 5.5. This change seems to be a result of an even larger fractional increase in d, without any significant change in b. This sample-to-sample variation does *not* reflect any model-fitting problems, since the symmetry parameter z is, on the average, somewhat closer to $\frac{1}{2}$ than in sample P07, and the fitting errors are *much* smaller.

The single run on sample P15 at 4.2 K produced an even larger transfer factor than in P07, and a d'/d ratio which has dropped to the remarkably low value of 0.01. It seems clear that this *uncycled* sample was under more strain than P07 was at 4.2 K, and had come closer to the one-valley, electronically hexagonal limit. The fitting error is small, and the symmetry parameter y is precisely $\frac{1}{2}$. On the other hand, the values of b, c, and d are extremely large. Such values might normally have indicated an inhomogeneous sample or some serious experimental disturbance, were they not accompanied by a very small longitudinal WFMR at 4.2 K and completely normal coefficients at 300 K. Moreover, the very large values of K and G extracted from the 4.2-K measurements make little or no sense within the framework of the conventional F-K-G model, despite the fact that the data fit the model so well. I defer the discussion of these peculiarities until Sec. V C.

3. Sample P16

Samples P15 and P16 were prepared from different portions of the same film. The carrier densities at 4.2 and 300 K (after cycling to 4.2 K) are practically identical in the two samples. The fitting errors and the deviations from $z=\frac{1}{2}$ are small for all of the eight room-temperature runs, and for seven of the eight, F lies in the rather narrow range 1.15—1.21. In particular, the three successive runs $300C$—$300E$ exhibit small and systematic changes (the calculated values of G, to *four* significant figures, are 1.135, 1.142, and 1.149) which may actually reflect a residual warming trend following the previous day's runs at 4.2 K. The explanation for the exceptional value $F=1.35$ in run $300B$ is unknown; more generally disturbing are the values of K, averaging 8.15, higher than the already high ones found in P15, as well as the G values, which are almost 5% higher, a substantial increase in this well-behaved parameter. It is of course a very subjective judgement, but these values are probably approaching the bounds of first-class sample quality and/or experimental technique. In this regard, the relatively low room-temperature mobility in sample P16 may be relevant.

For the first time, multiple runs were carried out at 4.2 K on this sample. Two pairs of runs were made on successive days, with a cycle to 300 K in between. Note the lower carrier mobility in the second pair, a consistently observed and very substantial effect of thermal cycling on properties *at helium temperatures.*[9] Much less weight should be assigned to the model parameter values from run $4A$ since this is the worst run mentioned earlier and shown in Fig. 5(a). Consequently, it is surprising, perhaps even disconcerting, that two of the fitted model parameters, F and G, are not very different from those extracted from the other three much improved runs which followed at this temperature. The overall values of K and G at 4.2 K are similar to those found in sample P15, and are therefore just as unrealistic. The F values are two orders of magnitude larger than any previously found at this temperature, but may not represent any significant physical difference, relative to sample P15. The problem here is the occurrence of negative values of d' which are not allowed by the F-K-G model. The only way that the computer program can reduce the rms error, almost entirely due to the difference in the experimental and computed values of d', is to make $d'=0$ ($F=\infty$). What is most significant about the results for sample P16 at 4.2 K, however, is that $|d'|/d$ remains small, of the order of 10^{-2}.

An intriguing and unique feature of the helium-temperature WFMR data in sample P16 is their downward trend in runs $4B$—$4D$, accompanied by downward trends in the model parameters as well. This could be some hard-to-pinpoint experimental problem which developed at 4.2 K, but it might also have some connection with the metastable low-temperature state which has been discovered in some doped IV-VI alloys.[60,61] The present samples were not deliberately doped, but the effects seen in doped samples are many orders of magnitude larger, so that it is just possible that the drift seen here is

the residual effect associated with a much lower, unintentional doping level.

4. Sample P22

This sample was the only one prepared at the Naval Surface Weapons Center (NSWC). The first two room-temperature runs suggest problems—note the G values, higher still than in P16. But then a sample lead popped off. After repairs, the next six runs at 300 K produced parameter values very similar to those found in the first film studied, P07, and therefore very similar to bulk values as well. The parameters from three runs at 77 K correspond to a slight increase in K and a 4% drop in G, relative to their values at 300 K. As noted earlier, this difference in the behavior of K as a function of temperature, as compared to that found in most bulk samples, may be a matter of the lower carrier density in the film. The change in G is precisely that found in the n-type bulk PbTe samples. The increase in F at 77 K to values exceeding 4 is in interesting contrast to the much smaller increase in thermally cycled sample P07. Section V D will reveal whether this larger effect is reasonable or not.

The run-to-run consistency in the sets of four WFMR coefficients obtained from the first five of six runs carried out on sample P22 at 4.2 K is very satisfying. In addition, these coefficients yielded values of K and G which are much closer to the reasonable range than those found in the other two high-F samples at 4.2 K. Furthermore, the symmetry parameter y is close to $\frac{1}{2}$, and the modest fitting errors are clearly correlated with the small but negative values of d', ($|d'|/d = 0.01$–0.02) rather than with any serious shortcoming. In particular, the run-to-run consistency in the K values is quite impressive, in view of the scatter found at *all* temperatures in many of the 48 runs. As indicated in Table V, the last run at 4.2 K was carried out (deliberately) at a Hall angle ($\sim 55°$) which is well outside of the weak-field range. The resulting changes in the WFMR coefficients and the model parameters are surprisingly modest, and there is no significant change in y or in the rms error E.

C. WFMR behavior and model fitting at 4.2 K

In this section, I will seek a better understanding of the WFMR behavior at 4.2 K. Our preview of the present results[11] focused on the results at this temperature and noted that in samples P15, P16, and P22, the overall behavior of the WFMR is strikingly different from that found in all previous WFMR data on PbTe, *including* the measurements on the *same three samples* at 77 K and above. It seems particularly illuminating to characterize the 4.2-K data in terms of the three standard configurations, M_1, M_1^2, and M_1^3 [Eqs. (20)–(22)], and d'. These four coefficients are summarized in Table VI for the twelve helium-temperature runs, with a reminder on the bottom line of how different these results are from typical room-temperature behavior (sample P22, run 300 K).

Because of the uncertainties and contradictions regarding the state of strain in epitaxial PbTe films, it is important to recognize what can be deduced from the general behavior of the 4.2-K WFMR even *before* any formal analysis is carried out. At the crystallographic level, there are no *a priori* constraints among d', M_1, M_1^2, and M_1^3 for the case of trigonal symmetry. But in three of the four samples, the experimental d'/d values have dropped to about 10^{-2}, indicating a close approach to hexagonal symmetry—a *crystallographic* condition that cannot be achieved by straining a cubic crystal. At the *electronic* level, the firmly established, no-strain starting point is the cubic $\langle 111 \rangle$ multivalley model. This model does not predict a small longitudinal WFMR in *any* crystallographic direction, simply because the symmetry axes of the different valleys are not aligned with one another. For example, with $K=4$ and $G=1$, the model predicts $M_1/M_1^3 = 0.75$. But experimentally, M_1 is much smaller, and the only way to account for this theoretically is to put most of the carriers into one valley. This carrier transfer can only result from an antibismuth type of trigonal dis-

TABLE VI. WFMR behavior at 4.2 K.

Sample number	Run	Standard WFMR configurations M_1	M_1^2	M_1^3	Skewness Coefficient d'
P07	4*A*	0.018	0.084	0.212	0.049
P15	4*C*	0.007	0.068	0.949	0.066
P16	4*A*	−0.045	−0.010	0.767	−0.058
	4*B*	0.014	0.066	0.967	−0.121
	4*C*	−0.001	0.051	0.798	−0.058
	4*D*	−0.002	0.053	0.667	−0.030
P22	4*C*	0.006	0.021	0.135	−0.004
	4*D*	0.008	0.022	0.135	−0.021
	4*E*	0.007	0.022	0.131	−0.022
	4*F*	0.008	0.023	0.135	−0.030
	4*G*	0.008	0.022	0.135	−0.030
	4*H*	0.008	0.018	0.106	−0.010
P22	300*K*[a]	0.198	0.290	0.357	0.356

[a]A room-temperature run, included to show the sharp contrast between 300- and 4.2-K data.

tortion along one of the ⟨111⟩ directions.

The conclusions from these general arguments regarding a close approach to a hexagonally symmetric one-valley model are quite firm, and they are reinforced by the high F values derived from the fit of the F-K-G model to the WFMR measurements at 4.2 K (Table V). But in all four samples, that fit produced values of G which were larger, not smaller, than at higher temperatures. This is generally not predicted by the F-K-G model for the case of a temperature-independent carrier density. In samples P15 and P16, moreover, both G and K have become unreasonably large at 4.2 K. These peculiar results suggest that some possible shortcomings of the model at low temperatures (see Sec. III) may have become significant.

Consequently, we investigated a low-temperature modification of the F-K-G model which seemed more realistic. We assumed $G=1$ (a good approximation at 4.2 K for the present samples), and introduced a new parameter

$$U=\mu_1/\mu_3 , \tag{28}$$

where μ_1 and μ_3 are any corresponding components of the mobility tensor in the single- and three-valley subsets of the ⟨111⟩ multivalley model. This parameter allows for the carrier-concentration dependence of the valley mobilities, another effect which should become important in strained crystals at low temperature, through the dependence of the scattering time on the Fermi levels in the valleys. The formulas for this F-K-U model are contained in Appendix B, and the best fits of the twelve helium-temperature runs produced the parameter values summarized in Table VII. The results are disappointing, and in some cases, the computer program did not produce a best-fit solution. A problem with all of the fits is that $U>1$. For the short-range defect scattering which predominates in PbTe at 4.2 K, it seems logical to expect carrier scattering rates to increase with increasing carrier density, and hence to expect $U<1$ for $F>1$.[62] The equations for this model contain U to the first, second, and third powers, but only the first power of F. It appears that the experimental data may be fitted more closely by simulating *carrier* transfer through *mobility* transfer.

With no other alternative models on the horizon, we returned to the F-K-G model and tried to find out why the experimental WFMR at 4.2 K in the three high-F samples led to such high values of K and G, and whether or not they could be understood within the framework of the model. First of all, we observed that for $F\gg1$, the expression for d' [Eqs. (A4) and (A7)] reduces to the particularly simple form

$$d'\approx[\tfrac{8}{9}(K-1)^2/K^2](G/F) . \tag{29}$$

This expression shows that d' is relatively insensitive to K, so that for *all* of the fitted values—K between 7 and 45 and G between 1.1 and 2.0—$d'=1/F$ to within a factor of 2. Hence, a very general connection between a small d' and a large F is predicted by the F-K-G model in the high-F range.

Next, we embarked on a long series of investigations of fitting-error contours in F-K space for a family of selected, constant-G values, using manufactured input sets of WFMR coefficients which deviated in various ways from perfect fits to the F-K-G model. We found that imperfect data could have large and sometimes strange effects on the best-fit solutions in the high-F region. We discovered "error troughs," which seemed to explain how solutions "leaked away" into the wrong F-K neighborhoods, but ultimately these error-contour studies did not provide the general insight into the origins of the problem that we had been seeking.

More recently, I decided to find out if a high-F approximation (constant terms plus terms linear in $1/F$) to the expressions for the WFMR coefficients in the F-K-G model (Appendix A) might become simple enough to reveal what was happening in that regime. The results, expressed in terms of the three standard coefficients, are

TABLE VII. Model parameter values for low-temperature transport (F-K-U) model, fitted to 4.2-K WFMR data.

Sample number	Run	Parameter values F	K	U	Error E[a] (10^{-2})
P07	4*A*	2.67	6.62	1.79	0.7
P15	4*C*	0.31	26.1	4.64	1.0
P16	4*A*	0.30	490	6.26	4.4
	4*B*	0.19	32.4	8.54	6.8
	4*C*	0.23	31.8	8.40	3.4
	4*D*	0.29	27.0	7.88	2.0
P22	4*C*	2.27	46.8	5.11	0.4
	4*D*	2.23	47.9	5.23	1.2
	4*E*	2.66	45.2	4.39	1.3
	4*F*	2.26	48.3	5.19	1.6
	4*G*	2.23	50.1	5.26	1.7
	4*H*	2.83	59.6	5.33	0.7

[a]rms difference between measured and calculated WFMR coefficients.

$$M_1 = \quad 0 \quad + \quad 0 \quad + \tfrac{12}{27} G(K-1)^2/K^2F \,, \tag{30}$$

$$M_1^2 = (G-1)/K + 4(G-1)(K-1)/K^2F + \tfrac{28}{27} G(K-1)^2/K^2F \,, \tag{31}$$

and

$$M_1^3 = G-1 \quad + \quad 0 \quad + \tfrac{32}{27} G(K-1)^2/K^2F \,. \tag{32}$$

This approximation does make it quite easy to identify the important relationships between the measured WFMR coefficients and the values of the model parameters. First of all, in the *strictly* one-valley limit ($F=\infty$), $M_1=0$, while[63]

$$K_1 = M_1^3/M_1^2 \tag{33}$$

and

$$G_1 = 1 + M_1^3 \,. \tag{34}$$

In this limit, G depends only on M_1^3; K is simply given by the ratio of the two transverse coefficients and is also equal to $\sigma_{\|}/\sigma_{\perp}$, the ratio of the conductivity in the film plane and normal to it. A better approximation to the solution of Eqs. (30)—(32) can be obtained by neglecting *only* the second term in Eq. (31). That term is smaller than the third term because it contains $G-1$, not G, and $K-1$, not $(K-1)^2$. Now M_1 is small, but not zero; the results for K and G remain simple, and are

$$K_2 = \frac{M_1^3 - \frac{8}{3} M_1}{M_1^2 - \frac{7}{3} M_1} \tag{35}$$

and

$$G_2 = 1 + M_1^3 - \tfrac{8}{3} M_1 \,. \tag{36}$$

The denominator of Eq. (35) immediately reveals that when M_1^2 is not very much larger than M_1, a small positive error in M_1 can lead to a large increase in the fitted value of K. But G has not changed much; it is still *almost* entirely determined by M_1^3, since $M_1 \ll M_1^3$ for the present experimental data (see Table VI).

Finally, the exact solution to Eqs. (30)—(32) is

$$K_3 = [A \pm (A^2 - 4K_2)^{1/2}]/2 \,, \tag{37}$$

where

$$A = 1 + K_2(1+g) \tag{38}$$

and

$$g = 9M_1/G_2 \,, \tag{39}$$

while

$$G_3 = G_2 \,. \tag{40}$$

According to Eq. (37), there are now two values of K which satisfy the high-F approximation to the F-K-G model. However, the smaller root of Eq. (37) corresponds to $F<1$, which violates the condition which originally led to Eqs. (30)—(32).

From the series of solutions, it becomes clear that when $F \gg 1$, K_1 can be a better approximation to K than K_2, when the denominator in Eq. (35) is seriously distorted by errors in the small coefficients M_1 and M_1^2. A second observation is that G ought to be a relatively stable and reliable parameter, since it is primarily determined by M_1^3, a much larger coefficient which is easiest to measure accurately. Not included in the above analysis is a third factor which connects experimental data to the model parameters, viz., the influence of d' on the best-fit values of K and G. Since $d' = 2M_1$ in the F-K-G model, a small positive or a negative measurement-derived d' can reduce the impact of an erroneously large M_1. On the other hand, it can increase parameter distortion if it is too large, relative to M_1.

The interplay between the WFMR data at 4.2 K and the model parameters may be seen by comparing the coefficients of Table VI with the model parameter values of Table VIII. The latter include K and G values for the three different solutions to the high-F approximation and those obtained from the full expressions for the F-K-G model.

The low value of K_1 for sample P07 most likely indicates that this least-strained film is not well described by the high-F approximation. In the case of sample P15, the values of K_1, K_2, and K_3 are more reasonable than the much larger K value. The trouble seems to lie with d' (which is not involved in the high-F approximation solutions); it is 9, rather than 2, times larger than M_1, and clearly has had a large impact on the best-fit parameters of the F-K-G model.

For samples P16 and P22, on the other hand, the much larger values of K_2 and K_3, relative to K_1, for run 4*B* of sample P16 and all runs of P22, indicate that M_1 is too large, relative to M_1^2, and is causing trouble in the denominator of Eq. (35). This problem is not present for runs 4*C* and 4*D* of sample P16 because M_1 is slightly negative in those two cases. But for all runs on samples P16 and P22, $K \approx K_1$, so that the predicted trouble never appears. Is seems clear that the unachievable negative values of d' are dominating the rms error and have thereby prevented complications.

The last important observation about Table VIII is that the sample-to-sample (and even run-to-run) variations in K and G, ranging from close-to-reasonable values of ~ 6 and 1.13 in sample P22 to the unreasonably high values of 12—33 and 1.67—1.96 in samples P15 and P16, are *correlated*.[64] Since the above analysis makes it quite clear that (except for run 4*B*, sample P16) K is not sensitive to variations in M_1 and M_1^2, the large values of *both* K and G must be primarily due to the accurately measured but anomalously large M_1^3. As it stands, the F-K-G model cannot account for this anomaly.

In our earlier letter,[11] we had observed that M_1^3 would be susceptible to enhancement by any kind of layering effect involving a carrier mobility which varied across the film thickness. One general possibility involves surface-related effects, such as surface-charge-induced band bending or an effectively layered mobility due to surface

TABLE VIII. High-F and exact solutions of F-K-G model for 4.2-K WFMR data.

Sample number	Run	High-F approximations[a] K_1	K_2	K_3	Exact K	High-F approximations[a] G_1	$G_{2,3}$	Exact G
P07	4*A*	2.52	3.90	4.59	4.27	1.21	1.16	1.16
P15	4*C*	14.0	17.9	18.5	32.6	1.95	1.93	1.89
P16	4*B*	14.7	28.2	30.1	16.1	1.97	1.93	1.96
	4*C*	15.6	15.6[b]	15.6[b]	15.9	1.80	1.80[b]	1.80
	4*D*	12.6	12.6[b]	12.6[b]	12.4	1.67	1.67[b]	1.67
P22	4*C*	6.43	17.0	17.9	7.24	1.13	1.12	1.13
	4*D*	6.14	38.0	40.5	7.17	1.13	1.11	1.13
	4*E*	5.95	18.7	20.3	6.98	1.13	1.11	1.13
	4*F*	5.87	28.5	30.4	7.14	1.13	1.11	1.13
	4*G*	6.14	38.0	40.5	7.19	1.13	1.11	1.13
	4*H*	5.89	∞[c]	∞[c]	7.24	1.11	1.09	1.10

[a]See Eqs. (30)—(40).

[b]These parameter values were obtained by assuming $M_1=0$ instead of using the negative value derived from the best fit of the WFMR to Eqs. (17)—(19).

[c]The actual calculated value of K_2 and K_3 would be a meaningless negative number, since for this run, $M_1^2 < \frac{7}{3}M_1$ [see Eq. (36)].

scattering and the large mean free path of the carriers at 4.2 K. But such effects ought to become more important in thinner samples, while experimentally, the least enhancement occurs in the thinnest film, sample P22.

We had therefore settled on the notion that in thicker samples, there would be an increased probability of finding a large *change* in the strain level between the substrate and opposite faces of the film.[11] Indeed, calculations have shown that for *perfectly elastic* films up to 30 μm in thickness, the variation in strain across the film thickness amounts to only a few percent or less.[25,32] But our earlier thermal cycling studies suggested that the generation of extended defects can lead to much more substantial effects in real films.[9] Isotropic, two-layer theoretical models[65,66] do predict enhancement of the transverse WFMR coefficient corresponding to M_1^3. Experimental enhancements up to a factor of 5 were actually found in PbS films.[67]

One final comment about these anomalies in the low-temperature results is essential: They are *not* explainable in terms of random electrical inhomogeneities in the films. Such inhomogeneities will produce $\vec{B}$-dependent distortions in current paths which are generally expected to enhance magnetoresistance. The extremely small values of longitudinal WFMR seen at 4.2 K—actually zero, within experimental error, for most of the runs—would never have been found in samples with significant inhomogeneity problems.

D. Carrier transfer, intervalley energy shifts, and film strain

To begin this final section of discussion, I will use the values of F derived from the F-K-G model fit to evaluate the shift in the band-edge energy of the strain-axis valley (T) relative to that of the other three (L) valleys. The results obtained will be compared to energy shifts determined from other kinds of measurements. The corresponding strains, determined from the shear deformation-potential constant, will be compared with results obtained from x-ray studies carried out elsewhere. And finally, the *changes* in the strains as a function of temperature will be compared with those expected from the difference in the thermal expansion coefficients of the film and substrate. In keeping with the remarks made in the previous section, note that these values are averages of quantities that may vary considerably across the film thickness in some of the present samples.

The intervalley band-edge energy shift may be defined as

$$\Delta E_c = E_c(L) - E_c(T) , \tag{41}$$

so that a positive ΔE_c corresponds to $F>1$. I determined n_1 and n_3 from $F=n_1/n_3$ and $n=n_1+3n_3$, where n is the total carrier density deduced from the strong-field Hall coefficient at 4.2 K. The Fermi energies for n_1 and n_3 carriers were then obtained from the standard formula for a single ellipsoidal parabolic valley,

$$n_{1,3} = 4\pi(2m_t^{2/3}m_l^{1/3}kT/h^2)^{3/2}F_{1/2}[E_F(T,L)/kT] , \tag{42}$$

where m_t and m_l are the transverse and longitudinal masses characterizing the valley, k and h are Boltzmann's and Planck's constants, E_F and T are the Fermi energy and absolute temperature, and $F_{1/2}(\eta)$ is the Fermi-Dirac function

$$F_{1/2}(\eta) = \int_0^\infty \frac{x^{1/2}dx}{1+\exp(x-\eta)} , \tag{43}$$

where $\eta = E_F/kT$ and $x = E/kT$. For the PbTe conduction-band parameters[48] $m_t=0.024$ and $m_l=10m_t$, Eq. (42) becomes

$$n_{1,3} = 6.40\times10^{13}T^{3/2}F_{1/2}(\eta_{T,L}) \tag{44}$$

in units of cm^{-3}. Finally, ΔE_c is just the difference $E_F(T)-E_F(L)$.

In the limit of classical statistics, ΔE_c no longer depends on the band parameters, and it is directly related to F by

$$\Delta E_c = kT \ln F \ . \tag{45}$$

For the present samples at room temperature, this simple formula yielded values of ΔE_c which agree with those obtained from the double application of Eq. (42), to better than 1%. On the other hand, the degenerate limit becomes a good approximation for the present samples at 4.2 K; then

$$E_F(0) = (h^2/2m_t^{2/3}m_l^{1/3})(3n_{1,3}/8\pi)^{2/3} \ . \tag{46}$$

For the PbTe parameters quoted above, this becomes

$$E_F(0) = 7.05\times 10^{-11} n_{1,3}^{2/3} \tag{47}$$

in units of meV.

As Table V shows, most of the room-temperature WFMR measurements correspond to $F = 1.0$—1.2. For an average value of 1.1, the analysis described above yields $\Delta E_c = 2.5$ meV. In the case of the final three room-temperature runs on much-cycled sample P07, I estimate that $F = 1.00 \pm 0.02$, indicating a zero energy shift within an uncertainty of ± 0.5 meV. When data of the quality of those included in Table V are available, I estimate that this kind of analysis can detect band-edge energy shifts as small as 1 or 2 meV.

From the WFMR measurements at 77 K, I used the three runs made on sample P22. For n(total) $= 7.6\times 10^{16}$ cm^{-3} and F(average) $= 4.7$, $\Delta E_c = 12.6$ meV. At 4.2 K, the WFMR in samples P15, P16, and P22 [$n = (6$—$8)\times 10^{16}$ cm^{-3}] suggests that essentially all of the carriers have been transferred to the single valley along the strain axis. This requires an intervalley energy shift of at least 11—13 meV. Complete transfer at 4.2 K was also deduced from Shubnikov—de Haas measurements on two n-type PbTe samples with carrier densities within this range.[22,28] In the case of sample P07, it appears that carrier transfer was not quite complete at 4.2 K. The value $F = 12.7$ yielded $\Delta E_c = 12.6$ meV, whereas complete transfer (at this sample's somewhat higher carrier concentration of 9.9×10^{16} cm^{-3}) would require a shift of 15.1 meV or more.

In sharp contrast to these low-temperature dc magneto-transport measurements, all of the magneto-optical data at 4.2 K have yielded much smaller, even undetectably small, values of ΔE_c.[25,29,33,68—70] For example, a study of far-infrared magnetophotoconductivity produced a complex structure in the magnetic field dependence which was very sensitive to ΔE_c. The best-fit value was found to be 1.8 ± 0.2 meV.[29] Two other recent studies of interband magneto-optical transitions concluded that the forbidden energy gaps at T and L differ by only 1 or 2 meV.[25,33] According to Ferreira's calculations,[23] this corresponds to a ΔE_c of about 4 or 8 meV.

The second step is to estimate the film strains corresponding to the intervalley energy shifts quoted above. The strains were obtained from the relation

$$\Delta E_c = 1.85 \Xi_u \epsilon_{11}^f \tag{48}$$

(in units of eV), where Ξ_u is the shear deformation-potential constant, as defined by Herring and Vogt,[71] and ϵ_{11}^f is one of the two equal in-plane components of strain in the film-oriented coordinate system of Fig. 1. The rather tedious process involved in evaluating the numerical coefficient in Eq. (48) is outlined in Appendix C. The calculated value of Ξ_u is 8.29 eV,[23] while lower experimental values of 3 and 4.5 eV were reported some time ago.[72] In a very recent study, the still lower value of 2.09 eV (25% of the original calculated value) was invoked and justified.[73] For reasons to be explained below, I used 4.15 eV, half the calculated value, in Eq. (48).

For the average room-temperature shift of 2.5 meV, $\epsilon_{11}^f = 3.2\times 10^{-4}$. For sample P07 in its final, essentially unstrained condition at 300 K, the uncertainty of ± 0.5 meV corresponds to a zero strain, within $\pm 6\times 10^{-5}$. These uncertainty limits would be halved or doubled, if I had used the largest or smallest values of Ξ_u cited above. Hohnke and Hurley,[31] in their x-ray study of (111)-oriented PbTe deposited on either BaF_2 or SrF_2, had detected no strain in the PbTe film to within $\pm 3\times 10^{-5}$. On the other hand, the more recent x-ray studies of PbTe on BaF_2 at room temperature by Fantner *et al.*[32,33] found *compressive* strains in the range $-(0.3$—$1.0)\times 10^{-3}$. They ascribed this compression to the elastic accommodation of up to about 3% of the 4% lattice mismatch between PbTe and BaF_2.

The average value $\Delta E_c = 12.6$ meV from the three runs on sample P22 at 77 K corresponds to $\epsilon_{11}^f = 1.6\times 10^{-3}$. Fantner has also compared the temperature evolution of the lattice parameters of PbTe films on BaF_2 with that of bulk PbTe. In one film, this comparison allowed him to deduce a compressive strain of -1.3×10^{-3} at 300 K, no strain near 110 K, and a tensile strain of roughly 5×10^{-4} at 77 K.[74] The values $\Delta E_c = 11$—13 meV needed to explain complete carrier transfer at 4.2 K for the present samples [with $n = (6$—$8)\times 10^{16}$ cm^{-3}] correspond to strains of at least $(1.6$—$1.8)\times 10^{-3}$. If I apply the same value of Ξ_u, 4.15 eV, to the 4.2-K magneto-optical data cited above, the strains lie in the range $(0.3$—$1.2)\times 10^{-3}$.

Figure 7 summarizes the strains measured or deduced

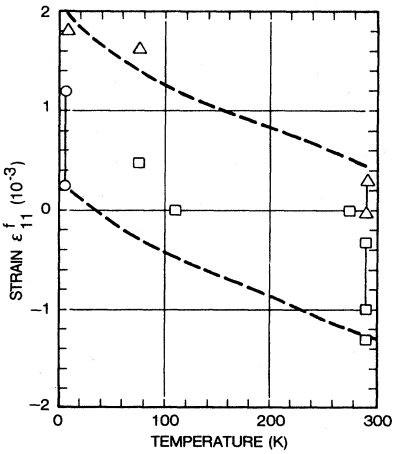

FIG. 7. In-plane film strain component ϵ_{11}^f as a function of temperature, derived from transport (△), x-ray (□), and magneto-optical (○) measurements. Dashed lines indicate the *changes* in strain expected from the PbTe/BaF_2 thermal-expansion coefficient difference.

for PbTe at various temperatures. Superimposed on this figure are dashed lines which indicate how two arbitrarily chosen strains would *change* with temperature, due to the difference in thermal-expansion coefficients of PbTe and BaF_2, integrated over the temperature intervals of interest.[75] The lines drawn correspond to the usual approximation, appropriate when the substrate is much thicker than the film, that *all* of this difference appears as strain in the film. When cooled below room temperature, unstrained PbTe always contracts faster than BaF_2. Thus when the PbTe on BaF_2 is cooled, the change in strain of the PbTe film will always be positive. For the cooling intervals 300—77 and 300—4.2 K, the expected positive changes are[75] 0.96×10^{-3} and 1.55×10^{-3}.

Since the dashed lines assume that all of the strain appears in the PbTe film, and make no allowance for any inelastic relaxation that may occur, they are an estimate of the largest possible change. Had I chosen to use a smaller Ξ_u than 4.15 eV, the changes in strain with temperature, deduced from the magnetoresistance measurements, would have exceeded this maximum. Note also that the changes in strain derived from Fantner's lattice-constant measurements[74] at 300 (the lowest square at this temperature in Fig. 7), 110, and 77 K also exceed this estimated maximum significantly.[74,76]

The main message to be extracted from Fig. 7 is that at any given temperature there are large differences in the strains obtained from different measurements, and even from the same kind of measurement on different samples. This is not surprising, in view of our earlier finding that thermal cycling has a substantial effect on the physical and electrical properties of PbTe films deposited on BaF_2.[9] A number of the publications relating to strain in PbTe/BaF_2 have included a discussion of the factors which affect the level of strain in the PbTe film, as well as the strain variations across the film thickness.[22,24–26,31,32] But in my view, a clear and consistent picture which relates these factors to the state of strain has not yet emerged. What is most puzzling about the present WFMR measurements is the lack of any indication of compressive strain at 300 K, in any of the four samples studied. Three of those samples were prepared by Lopez-Otero, who had also grown the films for the x-ray studies.[32,33] There is a possible explanation for the significant difference between the results of optical and transport measurements. The processing needed to transform an optical sample into a "Hall bar" suitable for magnetoresistance measurements has been found to alter the film strain appreciably.[77]

I hope that some individual or group has the interest and stamina to undertake a systematic study in which various kinds of measurements mentioned in the present paper are carried out in succession on a given sample, and are studied as a function of various sample growth parameters and post-growth thermal histories.

VI. SUMMARY AND CONCLUSIONS

In this paper, a very long series of WFMR measurements, using a newly developed four-coefficient technique, were discussed and analyzed. The close conformity of almost all of the data to the general constraints imposed by the definition of WFMR and by crystal symmetry attest to the high quality of the samples and the experimental technique. The latter benefited greatly from the use of an efficient computer-driven data-acquisition system.

The fourth WFMR coefficient makes it possible to distinguish between cubic and noncubic transport environments. The prediction that this new WFMR technique could become a convenient, reliable, and sensitive means to detect symmetry-lowering effects in semiconductor films is confirmed by the present study, which shows that strains as small as 1×10^{-4}, and perhaps smaller, can be measured. The strains actually deduced averaged around 2×10^{-4} at 300 K, and increased to nearly 1×10^{-3}, or more, at 77 K and lower temperatures. All measured strains correspond to in-plane stretching of the films. These results contrast strongly with x-ray studies which indicate in-plane *compressive* strains as large as -1.3×10^{-3} and also with most magneto-optical studies which suggest much smaller tensile strains at 4.2 K. The main reasons for these large variations seem to be differences in the growth parameters and thermal histories of the samples, but this is not a completely satisfactory explanation.

The WFMR measurements at 4.2 K represent the first complete sets (i.e., sufficient to determine three or four WFMR coefficients separately) ever obtained below 77 K, in *n*- or *p*-type PbTe, in bulk or thin-film form. Their characteristics, in three of the four samples studied, are very different from all previously published WFMR on PbTe. The symmetry of those low-temperature measurements corresponds to a close approach to an electronically hexagonal environment. Inevitably, this leads to the conclusion that substrate-induced strain has transferred all of the carriers into the single valley normal to the film plane.

Model fitting of the WFMR measurements at 4.2 K yielded some unusual values of the model parameters. These probably reflect the presence of a strain which varies across the film thickness, the variation becoming more important as the film thickness increases. This possibility was not investigated quantitatively, but it is clear that such a model does not invalidate the conclusion concerning complete carrier transfer to one valley at temperatures in the vicinity of 4.2 K.

The present measurements also reveal that the WFMR is sensitive to a number of different factors, and that there are large differences between the strains deduced from WFMR and from other kinds of data. If the full potential of this new four-coefficient technique is to be realized, it would be very desirable to carry out systematic, multiple-measurement studies on a set of PbTe films which are characterized by a range of growth parameters and post-growth thermal histories.

Note added in proof. The recent paper of Kriechbaum *et al.*[73] includes experimental data and an analysis based on the 4C WFMR technique.

ACKNOWLEDGMENTS

I am greatly indebted to the Naval Surface Weapons Center (from which I retired in 1981) for providing the

financial support for the preparation of this paper. My colleagues at NSWC—R. J. Abbundi, J. L. Davis, Bland Houston, Antonio Martinez, and J. B. Restorff—prepared samples, built apparatuses, developed computer programs, carried out experimental measurements, plotted and analyzed the results, and contributed in many other ways. Without their efforts there would have been no results for me to write about. My only regret is that they were not able to participate in the preparation of this manuscript.

I am also indebted to A. Lopez-Otero for providing NSWC with several high-quality PbTe films, and to G. Bauer, J. D. Dow, H. D. Drew, E. J. Fantner, H. Heinrich, H. Holloway, K. Lischka, S. W. McKnight, L. Palmetshofer, and D. L. Partin for stimulating discussions and written information concerning their work on the IV-VI semiconductors.

APPENDIX A: TRIGONALLY DISTORTED ⟨111⟩ MULTIVALLEY TRANSPORT MODEL (THE *F-K-G* MODEL)

The four WFMR coefficients for this model[8] are

$$b = 2X - Y \,, \tag{A1}$$

$$c = X - 2Y + Z \,, \tag{A2}$$

$$d = -6X + 6Y \,, \tag{A3}$$

and

$$d' = 2Z \,, \tag{A4}$$

where

$$X = \frac{3G[\frac{28}{27}(K-1)^2 + (F+3)K][(3F+5)K+4]}{K[(3F+1)K+8]^2} - \frac{[4K+(3F+5)]^2[(3F+5)K+4]}{[(3F+1)K+8]^2[8K+(3F+1)]} \,, \tag{A5}$$

$$Y = \frac{3G[\frac{32}{27}(K-1)^2 + (F-1)K^2 + 4K][(3F+5)K+4]}{K[(3F+1)K+8]^2} - 1 \,, \tag{A6}$$

and

$$Z = \frac{G[\frac{4}{3}(K-1)^2][(3F+5)K+4]}{K[(3F+1)K+8]^2} \,, \tag{A7}$$

The parameters F, K, and G are defined by Eqs. (12), (13), and (23).

APPENDIX B: LOW-TEMPERATURE MODIFICATION OF THE *F-K-G* TRANSPORT MODEL

In this model, F is unchanged, G is assumed to be unity, and a new parameter U [see Eq. (28)] is introduced which allows the carrier mobilities to depend on the carrier densities n_1 and n_3.

The results for the *F-K-G* model in Appendix A may be used to obtain the corresponding results for the present *F-K-U* model. Equations (A1)—(A4) remain the same. The parameter G is set equal to unity. In each of the square brackets of Eqs. (A5)—(A7), F should be replaced by FU^s, with $s = 1$, 2, or 3, as follows:

$$X\text{:}\ \frac{[3][1]}{[2]^2} - \frac{[2]^2[1]}{[2]^2[1]} \,, \tag{B1}$$

$$Y\text{:}\ \frac{[3][1]}{[2]^2} \,, \tag{B2}$$

$$Z\text{:}\ \frac{[*][1]}{[2]^2} \,. \tag{B3}$$

The bracket $[*]$ in Eq. (B3) does not contain F. See Eq. (A7).

APPENDIX C: RELATION BETWEEN INTERVALLEY BAND-EDGE ENERGY SHIFT AND STRAIN

The tedium involved in obtaining the numerical coefficient in Eq. (48) is almost entirely due to the need to transform second- and fourth-rank tensor components back and forth between the cubic-axis and film-oriented coordinate systems (Fig. 1) in which the WFMR coefficients are expressed. The latter set of coordinates will be identified by a superscript f.

To begin with, the shift δE of a band-edge energy due to strain may be expressed as

$$\delta E = \sum_{i,j} \Xi_{ij} \epsilon_{ij} \,, \tag{C1}$$

where Ξ_{ij} and ϵ_{ij} are the deformation-potential and strain tensors. In the cubic-axis coordinates,

$$\Xi_{ij} = \Xi_d \delta_{ij} + \Xi_u u_i u_j \tag{C2}$$

at the L points of the Brillouin zone, where u_i and u_j are the components of a unit tensor along the symmetry axis of the particular valley under consideration.[71] For the trigonal-axis (T) valley, with $u_1 = u_2 = u_3 = 1/\sqrt{3}$, combining Eqs. (C1) and (C2) yields

$$\delta E_T = \Xi_d(\epsilon_{11} + \epsilon_{22} + \epsilon_{33}) + \Xi_u[\tfrac{1}{3}(\epsilon_{11} + \epsilon_{22} + \epsilon_{33}) + \tfrac{2}{3}(\epsilon_{12} + \epsilon_{23} + \epsilon_{31})] \,. \tag{C3}$$

For one of the other (L) valleys, e.g., $[11\bar{1}]$, with $u_1 = u_2 = -u_3 = 1/\sqrt{3}$, the only change is the second part of the Ξ_u term which becomes $\frac{2}{3}(\epsilon_{12} - \epsilon_{23} - \epsilon_{31})$. Therefore the *difference* in conduction-band valley energy shifts is

$$\Delta E_c = \delta E_L - \delta E_T = -\tfrac{4}{3}\Xi_u(\epsilon_{23} + \epsilon_{31}) \,. \tag{C4}$$

In the film coordinates, the strain system is assumed to have the form $\epsilon^f_{11} = \epsilon^f_{22}$, $\epsilon^f_{33} \neq 0$ but different from ϵ^f_{11}, and $\epsilon^f_{ij} = 0$ for $i \neq j$. It is also assumed that there is no stress normal to the film plane, i.e., $\sigma^f_{33} = 0$. Therefore (switching to matrix notation)

$$\sigma_3^f = 0 = c_{31}^f \epsilon_1^f + c_{32}^f \epsilon_2^f + c_{33}^f \epsilon_3^f$$
$$= 2c_{31}^f \epsilon_1 + c_{33}^f \epsilon_3^f , \quad \text{(C5)}$$

where c_{ij}^f and ϵ_i^f are the components of the stiffness and strain matrices.[78]

The transformation matrix

$$\begin{array}{c|ccc} & x & y & z \\ 1 & 1/\sqrt{2} & -1/\sqrt{2} & 0 \\ 2 & 1/\sqrt{6} & 1/\sqrt{6} & -2/\sqrt{6} \\ 3 & 1/\sqrt{3} & 1/\sqrt{3} & 1/\sqrt{3} \end{array} \quad \text{(C6)}$$

must then be employed to express the c_{ij}^f in terms of the cubic axis c_{ij}, since measured stiffness coefficients are normally given in the cubic-axis system. Transforming the c_{ij}^f in Eq. (C5) leads to[79]

$$\epsilon_3^f = \frac{-2(c_{11}+2c_{12}-2c_{44})}{c_{11}+2c_{12}+4c_{44}} \epsilon_1^f . \quad \text{(C7)}$$

For the values $c_{11}=12.81$, $c_{12}=0.44$, and $c_{44}=1.514 \times 10^{11}$ dyn cm^{-2} obtained by Houston, Strakna, and Belson,[80] $\epsilon_3^f = -1.08\epsilon_1^f$. The quoted c_{ij} values are extrapolations to 0 K, but using 300-K values from the same paper produces only a 1% change in the numerical coefficient connecting ϵ_3^f and ϵ_1^f.

The strain components ϵ_{23} and ϵ_{31} in Eq. (C4) must next be expressed in terms of the film-coordinate strains ϵ_{11}^f and ϵ_{33}^f ($=\epsilon_1^f$ and ϵ_3^f). Again, using the transformation matrix, Eq. (C6), yields

$$\epsilon_{23} = \epsilon_{31} = -\tfrac{1}{3}\epsilon_{11}^f + \tfrac{1}{3}\epsilon_{33}^f . \quad \text{(C8)}$$

Expressing ϵ_{33}^f in terms of ϵ_{11}^f gives $\epsilon_{ij} = -0.693\epsilon_{11}^f$, so that, finally, Eq. (C4) becomes

$$\Delta E_c = \tfrac{8}{3} 0.693 \Xi_u \epsilon_{11}^f$$
$$= 1.85 \Xi_u \epsilon_{11}^f \quad \text{(C9)}$$

in units of eV. The numerical coefficient agrees with an earlier calculation by Lowney, Bis, and Foti.[81]

[1] A. C. Smith, J. F. Janak, and R. B. Adler, *Electronic Conduction in Solids* (McGraw-Hill, New York, 1967), Appendix C.

[2] A. C. Beer, *Galvanomagnetic Effects in Semiconductors* (Academic, New York, 1963), Chap. 8.

[3] In this paper, "we" refers to the accomplishments of my colleagues and myself, mostly prior to my 1981 retirement, while "I" identifies my own recent analyses and opinions, generated in the course of preparing the paper.

[4] R. S. Allgaier, J. B. Restorff, and Bland Houston, Appl. Phys. Lett. **34**, 158 (1979).

[5] R. S. Allgaier, J. B. Restorff, and Bland Houston, Phys. Rev. B **19**, 6155 (1979).

[6] R. S. Allgaier and J. B. Restorff, J. Appl. Phys. **50**, 402 (1979).

[7] R. S. Allgaier, J. B. Restorff, and Bland Houston, Phys. Rev. B **26**, 3449 (1982).

[8] R. S. Allgaier, J. B. Restorff, Bland Houston, J. D. Jensen, and A. Lopez-Otero, J. Appl. Phys. **51**, 2119 (1980).

[9] J. B. Restorff, R. S. Allgaier, and Bland Houston, J. Appl. Phys. **52**, 6185 (1981).

[10] A. Lopez-Otero, Thin Solid Films, **49**, 3 (1978).

[11] R. S. Allgaier, R. J. Abbundi, Bland Houston, J. L. Davis, A. Martinez, and J. B. Restorff, Appl. Phys. Lett. **41**, 941 (1981).

[12] Yu. I. Ravich, B. A. Efimova, and I. A. Smirnov, *Semiconducting Lead Chalcogenides* (Plenum, New York, 1970).

[13] K. Shogenji and S. Uchiyama, J. Phys. Soc. Jpn. **12**, 1164 (1957).

[14] R. S. Allgaier, Phys. Rev. **112**, 828 (1958).

[15] K. Shogenji, J. Phys. Soc. Jpn. **14**, 1360 (1959).

[16] R. S. Allgaier, in *Proceedings of the International Conference on Semiconductor Physics, Prague, 1960* (Czechoslovak Academy of Sciences, Prague, 1961), p. 1037.

[17] R. S. Allgaier, Phys. Rev. **119**, 554 (1960).

[18] J. N. Zemel, in *Solid State Surface Science,* edited by M. Green (Marcel Dekker, New York, 1969), Vol. 1, p. 291.

[19] H. Holloway, in *Physics of Thin Films,* edited by G. Haas and M. H. Francombe (Academic, New York, 1980), Vol. 11, p. 105.

[20] E. D. Palik, D. L. Mitchell, and J. N. Zemel, Phys. Rev. **135**, A763 (1964).

[21] D. L. Mitchell, E. D. Palik, and J. N. Zemel, in *Physics of Semiconductors—Proceedings of the 7th International Conference, Paris, 1964,* edited by M. Hulin (Dunod, Paris, 1964), p. 325.

[22] J. R. Burke and G. P. Carver, Phys. Rev. B **17**, 2719 (1978).

[23] L. G. Ferreira, Phys. Rev. **137**, A1601 (1965).

[24] G. P. Carver, Bland Houston, J. R. Burke, H. Heinrich, and A. Lopez-Otero, Solid State Commun. **30**, 461 (1979).

[25] H. Pascher, E. J. Fantner, G. Bauer, and A. Lopez-Otero, in *Physics in High Magnetic Fields, Proceedings of the Oji International Seminar, Hakone, Japan, 1980,* Vol. 24 of *Springer Series in Solid State Sciences,* edited by S. Chikazumi and M. Miura (Springer, Berlin, 1981), p. 244.

[26] A. Gungor, H. D. Drew, H. R. Verdun, and J. D. Jensen, Appl. Phys. Lett. **39**, 985 (1981).

[27] R. S. Allgaier, J. B. Restorff, and Bland Houston, J. Appl. Phys. **53**, 3110 (1982).

[28] D. V. Shamshur, R. V. Parfen'ev, D. V. Mashovets, A. V. Matveenko, V. V. Kosarev, and K. I. Geĭman, Fiz. Tekh. Poluprovodn. **16**, 1249 (1982) [Sov. Phys.—Semicond. **16**, 798 (1982)].

[29] A. Gungor and H. D. Drew, Solid State Commun. **44**, 701 (1982).

[30] Antonio Martinez and Bland Houston, Appl. Phys. Lett. **43**, 77 (1983).

[31] D. K. Hohnke and M. D. Hurley, J. Appl. Phys. **47**, 4975 (1976).

[32] E. J. Fantner, B. Ortner, W. Ruhs, and A. Lopez-Otero, in *Physics of Narrow Gap Semiconductors, Proceedings, Linz, Austria, 1981,* Vol. 152 of *Lecture Notes in Physics,* edited by E. Gornik, H. Heinrich, and L. Palmetshofer (Springer, Berlin, 1982), p. 59.

[33] E. J. Fantner, G. Bauer, W. Ruhs, B. Ortner, H. Pascher, and A. Lopez-Otero, Thin Solid Films **89**, 149 (1982).

[34] F. Seitz, Phys. Rev. **79**, 372 (1950).

[35] G. L. Pearson and H. Suhl, Phys. Rev. **83**, 768 (1951).

[36] Strictly speaking, this can be done by attaching another pair of

probes in the other, non-Hall transverse direction, in order to measure the so-called planar Hall coefficient. See A. C. Beer, *Galvanomagnetic Effects in Semiconductors,* Ref. 2, Chap. IV.

[37]B. Abeles and S. Meiboom, Phys. Rev. **95**, 31 (1954).

[38]M. Shibuya, Phys. Rev. **95**, 1385 (1954).

[39]R. S. Allgaier, Phys. Rev. **115**, 1185 (1959).

[40]There are actually two reciprocally-related solutions of Eqs. (15) and (16) for K (with corresponding G values), but the "oblate" ($K<1$) solution is rejected because it is not consistent with the known mass anisotropy.

[41]J. M. Brettell, J. Phys. D **1**, 1064 (1968).

[42]S. C. Gupta, K. N. S. Rajwanshi, and A. K. Sreedhar, Phys. Rev. B **15**, 2231 (1977).

[43]W. W. Scanlon, in *Solid State Physics,* edited by F. Seitz and D. Turnbull (Academic, New York, 1959), Vol. 9, p. 83.

[44]My own early WFMR measurements on p-type PbTe (Ref. 17) are themselves averages of results from six samples with very nearly identical characteristics.

[45]I used K and G values given in Ref. 17, but otherwise I calculated K and G from the published WFMR coefficient data. Because the data were so nearly consistent with the model, a least-squares fitting procedure was *not* used.

[46]With the exception of Brettell's measurements on a sample containing 2.5 at. % CdTe, Ref. 41.

[47]G. M. T. Foley and D. N. Langenberg, Phys. Rev. B **15**, 4850 (1977).

[48]S. W. McKnight and H. D. Drew, Phys. Rev. B **21**, 3447 (1980).

[49]O. S. Gryaznov and Yu. I. Ravich, Fiz. Tekh. Poluprovodn. **3**, 1310 (1969) [Sov. Phys.—Semicond. **3**, 1092 (1970)].

[50]E. H. Putley, Proc. Phys. Soc. London, Sect.. B **68**, 22 (1955).

[51]Y. Makino, J. Phys. Soc. Jpn. **19**, 1755 (1964).

[52]J. N. Zemel, J. D. Jensen, and R. B. Schoolar, Phys. Rev. **140**, A330 (1965).

[53]R. S. Allgaier, Bland Houston, and J. B. Restorff, J. Appl. Phys. **49**, 4442 (1978).

[54]A. Nishiyama, J. Phys. Soc. Jpn. **40**, 471 (1976).

[55]See Fig. 2 of Ref. 9.

[56]Yu. I. Ravich, B. A. Efimova, and I. A. Smirnov, *Semiconducting Lead Chalcogenides,* Ref. 12, p. 133.

[57]R. S. Allgaier, Proc. Soc. of Photo-Opt. Instrum. Eng. **285**, 2 (1981).

[58]D. Chattopadhyay and H. J. Queisser Rev. Mod. Phys. **53**, 745 (1981).

[59]G. Nimtz and B. Schlicht, in *Narrow-Gap Semiconductors,* Vol. 98 of *Springer Tracts in Modern Physics,* edited by G. Höhler and E. A. Niekisch (Springer, Berlin, 1983), p. 1.

[60]B. A. Akimov, N. B. Brandt, S. A. Bogoslovskii, L. I. Ryabova, and S. M. Chudinov, Pis'ma Zh. Eksp. Teor. Fiz. **29**, 11 (1979) [JETP Lett. **29**, 9 (1979)].

[61]B. M. Vul, I. D. Voronova, G. A. Kalyuzhnaya, T. S. Mamedov, and T. Sh. Ragimova, Pis'ma Zh. Eksp. Teor. Fiz. **29**, 21 (1979) [JETP Lett. **29**, 18 (1979)].

[62]This expectation is in accord with the observation that the defect-limited carrier mobility in PbTe and SnTe decreases faster than the reciprocal of the carrier density. See R. S. Allgaier and B. B. Houston, in *Report of the International Conference on the Physics of Semiconductors, Exeter, 1962* edited by A. C. Stickland (IOP, London, 1962), p. 172.

[63]I use subscripts 1, 2, and 3 on K and G to identify a series of increasingly accurate approximations to the solution of Eqs. (30)—(32) for these two model parameters.

[64]The quoted ranges exclude the values from run 4A on sample P16, since they were obtained from a fit to a completely negative in-plane WFMR.

[65]A. Nedoluha and K. M. Koch, Z. Phys. **132**, 608 (1952).

[66]R. L. Petritz, Phys. Rev. **110**, 1254 (1958).

[67]M. H. Brodsky and R. B. Schoolar, J. Appl. Phys. **40**, 107 (1969).

[68]H. Burkhard, G. Bauer, P. Grosse, and A. Lopez-Otero, in *Physics of Semiconductors, Proceedings of the 13th International Conference, Rome, 1976,* edited by F. G. Fumi (North-Holland, Amsterdam, 1976), p. 439.

[69]H. Burkhard, G. Bauer, P. Grosse, and A. Lopez-Otero, Physica B **89**, 22 (1977).

[70]H. Burkhard, G. Bauer, and W. Zawadzki, Phys. Rev. B **19**, 5149 (1979).

[71]C. Herring and E. Vogt, Phys. Rev. **101**, 944 (1956).

[72]Yu. I. Ravich, B. A. Efimova, and I. A. Smirnov, *Semiconducting Lead Chalcogenides,* Ref. 12. p. 138.

[73]M. Kriechbaum, K. E. Ambrosch, E. J. Fantner, H. Clemens, and G. Bauer, Phys. Rev. B **30**, 3394 (1984).

[74]E. J. Fantner, private communication.

[75]R. F. Bis (unpublished).

[76]Note that some of the data in Fig. 7 are actually the published values of ϵ_{33}^{f}, which is 8% larger in magnitude than ϵ_{11}^{f} (see Appendix C).

[77]G. Bauer, private communication.

[78]The matrix conventions used are those given in J. F. Nye, *Physical Properties of Crystals* (Clarendon, Oxford, 1957), Chaps. VII and VIII.

[79]Note the error in the corresponding expression, Eq. (2) of E. J. Fantner, B. Ortner, W. Ruhs, and A. Lopez-Otero, in *Physics of Narrow Gap Semiconductors,* Ref. 32, p. 62.

[80]Bland Houston, R. E. Strakna, and Henry S. Belson, J. Appl. Phys. **39**, 3913 (1968).

[81]J. R. Lowney, R. F. Bis, and S. C. Foti, Naval Surface Weapons Center (White Oak Lab) Technical Report No. 78-5 (unpublished).